Predicting co-contraction with an open source musculoskeletal shoulder model during dynamic and static tasks

Predicting co-contraction with an open source musculoskeletal shoulder model

during dynamic and static tasks

By

Spencer M. Savoie, B.Sc.

A Thesis Submitted to School of Graduate Studies in

Partial Fulfillment of the Requirements for the Degree

Master of Science

McMaster University
Hamilton, Ontario

MASTER OF SCIENCE (2014) McMaster University

(Kinesiology) Hamilton, Ontario

TITLE: Predicting co-contraction with an open source musculoskeletal shoulder model during dynamic and static tasks

AUTHOR: Spencer M. Savoie, B.Sc. (McMaster University)

SUPERVISOR: Dr. Peter J. Keir

NUMBER OF PAGES: viii, 99

ABSTRACT

The shoulder is one of the most complex joints in the body. It has a large range of motion and has active, as well as passive, components to its stabilization. Many injuries occur every year due to overexertion and strain on the shoulder. Musculoskeletal models can be used as a proactive ergonomics tool for shoulder specific job task design, and to help prevent these injuries before they occur. The purpose of this thesis was to critically evaluate the performance of four optimization criteria (sum of squared activation, sum of cubed activation, sum of quartic activation, and entropy assisted) using the open source modeling platform OpenSIM. Experimental torque, kinematic, and EMG data were collected using ten participants for a variety of dynamic arm movements, and static arm postures, in different planes of action. The kinematic and torque data were processed and used as inputs to OpenSIM to calculate predicted muscle activations and joint reaction forces. Experimental EMG was cross correlated with the predicted muscle activity of 8 muscles, and RMSD was calculated between experimental and predicted muscle activity for evaluation. A co-contraction index was also used to assess the model's ability to predict co-activation between muscle pairs. Overall, the sum of cubed activation and sum of quartic activation model predictions explained significantly more variance ($38 \pm 2.5\%$, $p<0.01$) than the sum of squares and entropy models, when compared with experimental EMG. In conclusion, the type of optimization criterion chosen had an effect on the accuracy of the model predictions. Future research, in the development of optimization criterions for the shoulder, will create better model predictions of muscle

forces and joint reaction forces, enabling musculoskeletal models to be more useful as a tool to the clinical and ergonomic populations.

ACKNOWLEDGEMENTS

It goes without saying, I would not have been able to complete this thesis without the support from my committee, family, and friends. My sincerest gratitude goes to my supervisor Dr. Peter Keir as well as my committee members Dr. Jim Potvin and Krista Madsen. The immense knowledge, care, and mentorship from Dr. Peter Keir helped me overcome all setbacks as well as provide the best research environment there is. Dr. Jim Potvin and Krista Madsen provided excellent guidance and patience, which greatly impacted the depth and quality of this thesis. My thanks and appreciations also go out to my lab mates and colleagues who have helped me to the best of their ability over the course of this thesis.

To my friends and lab mates, I have spent six years at McMaster and these past two rival my best. The memories from all of the trips and events will not soon be forgotten. Frequent trips to the Phoenix, Heimbecker, and all grad events were always a well needed break from studies. To my family, I would not have even made it through undergrad without your support. Your ongoing love, guidance, and encouragement have never weakened and have helped me throughout my life and this thesis. My deepest appreciation goes to all those that have helped me on this journey.

TABLE OF CONTENTS

ABSTRACT -- i

ACKNOWLEDGEMENTS -- iii

LIST OF FIGURES -- vi

LIST OF TABLES --- ix

CHAPTER 1. INTRODUCTION -- 1

CHAPTER 2. REVIEW OF LITERATURE ---------------------------------- 4

2.1. Shoulder Anatomy & Stability ------------------------------------ 4

2.2. Incidence & Risk of Workplace Shoulder Injuries ---------------- 9

2.3. Biomechanical Shoulder Models ------------------------------------ 11

2.4. Model Validation Techniques --------------------------------------- 21

2.5. Purpose -- 23

2.6. Hypotheses -- 23

CHAPTER 3. METHODS --- 24

3.1. Data Acquisition -- 24

3.1.1. Participants -- 24

3.1.2. Collection Protocol -- 24

3.1.3. Apparatus & Instruments ---------------------------------- 30

3.2. Data Analysis -- 35

3.2.1. Kinematics & EMG processing --------------------------- 35

3.2.2. Scaling, Inverse Kinematics, & Static Optimization --- 36

3.2.3. Muscle Matching & Co-Contraction Index ------------- 39

3.3. Statistics -- 40

3.4. On Creating a Novel Shear Force Optimization Criterion ------- 43

CHAPTER 4. RESULTS -- 45

4.1. Model Summary -- 45

4.2. EMG & Model Evaluation -- 47

4.3. Co-Contraction Index-- 55

4.4. Joint Reaction Force -- 58

CHAPTER 5. DISCUSSION --- 61

5.1. Model Summary -- 61

5.2. Co-Activation --- 65

5.3. Joint Reaction Force -- 67

5.4. Limitations --- 71

5.5. Future Directions -- 74

5.6. Conclusion -- 76

REFERENCES -- 78

APPENDIX A: Normalized EMG for All Muscles and All Conditions ----- 91

APPENDIX B: MREB Certificate of Ethics Clearance -------------------------- 95

APPENDIX C: Participant Letter of Consent Form ------------------------------- 96

LIST OF FIGURES

Figure 1. Average maximum translating force resisted in 8 directions (0°= superior, 90°= anterior) with a humeral head compression into the glenoid concavity of 50 N (Lippitt & Matsen, 1993). -- 5

Figure 2. Overhead view of glenoid fossa and humerus. A) Glenoid centre is perpendicular to the midpoint of the glenoid concavity in an axis. B) Stable joint. C) Unstable joint since the joint reaction force is not directed into the cavity. D) Unstable joint due to abnormal glenoid version (Lippitt & Matsen, 1993). -- 6

Figure 3. Average stability ratios for 13 shoulder muscles and muscle sub regions during arm flexion. Ratios between 1 & -1 are deemed stable (Ackland & Pandy, 2009). -- 8

Figure 4. WSIB High Impact Claims during 2012, 6.3% of all claims were high impact shoulder claims (WSIB, 2013). --- 10

Figure 5. Mollier 1899 Shoulder Muscle Model (from Van Der Helm, 1994a). -- 12

Figure 6. Glenohumeral stability constraint, c_i = the ratio coefficient in the i^{th} direction, $F_{s,i}$= shear force acting in the i^{th} direction, F_c= compressive force directed into glenoid cavity (adapted from Dickerson et al, 2007). ---------------- 14

Figure 7. DSM Finite Element Model Right Shoulder Complex (not all muscles and ligaments shown)(Van der Helm 1994a). ------------------------------ 15

Figure 8. Estimated muscle forces (chart) and glenohumeral JRF position within glenoid (circle) during a supraspinatus tear (A) and a supraspinatus and infraspinatus tear (B) for constrained and unconstrained conditions (Steenbrink et al, 2009). --- 21

Figure 9. Postures for protocol, a; top down view of three different planes of action. b; 2 different elevation angles. Black straps and arrows designate positions and approximate direction of the force application. ----------------------- 26

Figure 10. Glenohumeral stress test (apprehension position). ----------------- 27

Figure 11. Snapshot of visual feedback animation on monitor during dynamic trials. The blue bar (arm) would rotate back and forth through the described range of motion (annotated by red arrows) to mimic flexion and extension. Metronome tones were audible when the blue bar passed a black line representing either 0%, 50%, or 100% completion of the prescribed range of the motion. -- 28

Figure 12. Biodex setup with pad attachment during sagittal plane flexion movement. 1) Biodex System 4 dynamometer, 2) custom arm attachment and pad, 3) custom foam spacer, 4) foot rest, 5) torso strap. -------------------------------- 31

Figure 13. The process of analysis in OpenSIM to obtain muscle and joint reaction forces. --- 36

Figure 14. OpenSIM DSEM model with bones, virtual marker set (6 pink spheres), and thoracic wrap object (blue mesh). -------------------------------------- 37

Figure 15. Scapular Reference Frame in OpenSIM. Z and Y joint reaction force components are shear, X joint reaction force component is compression. --- 38

Figure 16. Subject 5 normalized EMG recordings in the sagittal plane for the conditions; *a*) stress test, *b*) dynamic 120°/s, *c*) dynamic 60°/s, *d*) static 60°, *e*) static 120°. Each chart illustrates the recorded muscle activations over the duration of the trial. --- 49

Figure 17. Mean explained variance for all tasks between experimental and predicted muscle activations for each muscle within each model (error bars represent standard error). -- 50

Figure 18. Overall Mean RMSD between experimental and predicted muscle activations for each muscle within each model (errors bars represent standard error). Major agonists include the anterior deltoid, and pectoralis major. Minor agonists include middle deltoid, trapezius, and supraspinatus. ---------------- 52

Figure 19. Mean of all muscles explained variance for each model during each condition. (error bars represent standard error). ----------------------------------- 54

Figure 20. Mean of all muscles RMSD between experimental and prediction muscle activity of all muscles in each condition for each model (error bars represent standard error). -- 55

Figure 21. Predicted and experimental CCI with standard error for all 12 muscle pairs; PEC= pectoralis major, INFRA= infraspinatus, LD= latissimus dorsi, PD= posterior deltoid, AD= anterior deltoid, MD= middle deltoid (error bars represent standard error). -- 56

Figure 22. Average CCI and standard error of muscle pairs for each condition; PEC= pectoralis major, INFRA= infraspinatus, LD= latissimus dorsi, PD= posterior deltoid, AD= anterior deltoid, MD= middle deltoid (error bars represent standard error). -- 57

Figure 23. Mean resultant JRFs for sum of activation models and entropy-assisted model over duration of slow flexion trial (shadow represents standard error). -- 58

Figure 24. The average stability ratio (SR) and standard deviation of each condition as well as direction of shear force (*θ)* and standard deviation; *b*) Fast, *c*) Slow, *d*) Static 60°, *e*) Static 120°, *f*) Stress Test. The grey oval represents the dislocation threshold (threshold levels described in *a*)., the red ring represents the conditions average SR, and the arrow represents the direction of the shear force. Note, the static 120° SR is not seen to scale as it is much larger than the other ratios. -- 60

Figure 25. Normalized experimental and predicted muscle activations for each model and each trial condition (*a,b,c,d,e*) averaged across all participants. The experimental activation traces are shadowed with the standard error. (*a*) The average activation of all fast trials over the duration of the recorded movement (0%=0°, 100%= 135°). (*b*) the average activations of all slow trials, (*c*) the average activations of stress test, (*d*) average activations of static 60° trials, and (*e*) average activations of static 120°. -------------------------------- 63

Figure 26. Resultant JRFs presented with standard error for *a*) the sum of activation models, and *b*) the entropy model, during slow shoulder flexion. The average sum of activation squared model for slow trials (green) *c*) is overlaid on results from *in vivo* JRF measurements as well as three different models from Nikooyan et al. (2010). The symbol (N) designates results are from Nikooyan et al (2010). -- 71

LIST OF TABLES

Table 1: Summary of trials. --- 27

Table 2: Summary of actions used to elicit isometric and dynamic MVC's in recorded muscles. -- 30

Table 3: Electrode placements and test maneuvers (adapted from Perotto et al, 2005) -- 34

Table 4: Corresponding muscle elements for each recorded muscle. --------- 39

Table 5: Muscle pairs used for calculation of co-contraction index. ---------- 40

Table 6: Participant anthropometrics (mean with standard deviation). ------- 45

Table 7: Mean RMSD and mean, maximum, and minimum explained variance for each model presented with standard deviation. ------------------------ 47

Table 8: Average correlation coefficients for all trials compared to literature. -- 65

1. INTRODUCTION

The upper extremity is essential to completing most tasks in the workplace. However, the reliance on the shoulder to carry out these tasks comes with a cost. In 2013, Ontario had 2568 injury claims reported for the shoulder (6.2% of all claims), and 95% of which were considered “high impact” claims. High impact claims are associated with slower recovery times, longer return to work times, higher costs to the employer, and are most commonly caused by overexertion (WSIB, 2013). To reduce upper extremity injuries in the workplace, proactive ergonomic tools can be used to design safer working tasks before they are implemented into the workplace and before injuries occur. Some proactive ergonomic tools rely on models and simulations to determine safe working levels, thus improving on modeling of the shoulder will allow better predictions of worker capabilities for the upper body (Högfors et al, 1995; Chaffin, 2005).

The shoulder complex represents a fine balance of stability and mobility. This combination leads to strain at the shoulder from overexertion or functional overload. Functional overload may be described as the point in which muscle damage occurs due to overexertion (Folland et al, 2000). Overexertion occurs when the forces required to complete a task exceed a given tissue’s tolerance. Repetitive functional overload can lead to conditions such as chronic inflammation and impingement which can eventually cause instability at the shoulder joint (Morrison et al, 2000). Chronic instability may also lead to inflammation and risk for injury (Warner et al, 1990), creating a vicious cycle. The shoulder joint complex is stabilized by the labrum, glenohumeral and coracohumeral ligaments, as well as the surrounding musculature. The labrum and ligaments support the shoulder joint passively, while the surrounding musculature supports it actively. Muscles create forces that prevent translation of the humeral head in the glenoid fossa (Culham and Peat, 1993), but as these muscles fatigue, there is less dynamic support and increased possibility for excessive translational instability at the shoulder joint (Itoi et al, 2000).

Similar to a ball and socket, the joint is most stable with compression forces directed through the centre of the joint and less stable when the force has a large shear component that promotes translation of the ball within the socket (Poppen & Walker, 1978). The glenohumeral joint requires the surrounding musculature to reduce the net shear strain at the joint and limit translation of the humeral head (Lee et al, 2000). If biomechanical models of the shoulder are to accurately represent (the anatomy and) function they must account for shear forces at the joint.

Several complex models have been developed for the shoulder joint, the Karlsson and Peterson model (1992), Holzbaur et al model (2005), Dickerson et al model (2007), and the Delft Shoulder and Elbow Model (DSEM) (Van der Helm, 1994a,1994b). The DSEM is available through open source musculoskeletal modeling software (OpenSIM). This software enables the development and modification of musculoskeletal models which use inputs of kinematics and forces to predict individual muscle activation and force (Delp & Loan, 1995). Similar to other musculoskeletal models, the DSEM contains multiple optimization functions and constraints which may be manipulated to better represent both anatomy and function (Van der Helm, 1994a).

The purpose of this thesis was to investigate the performance of several different optimization functions using the DSEM upper extremity model implemented in OpenSIM and, secondly, to observe the possibility of predicting co-contraction occurring at the shoulder complex. These empirical comparisons were based on the model's predicted muscle activity compared to experimental EMG collected under conditions designed to test specific features of the model.

2. REVIEW OF LITERATURE

2.1 Shoulder Anatomy and Stability

The shoulder complex consists of the humerus, scapula, clavicle, sternum, and thorax which form four joints to produce a large multiaxial range of motion (Inman et al 1944). The scapulothoracic, sternoclavicular, and acromioclavicular joints play a role in shoulder movement but most of the motion occurs at the glenohumeral (GH) joint. The GH joint can be described as a synovial ball and socket joint between the humeral head and the glenoid fossa of the scapula (Culham & Peat, 1993). The humeral head has a surface area approximately 3 times larger than the fossa and therefore needs additional structures to stabilize the joint (Saha, 1971).

Shoulder mobility is a tradeoff between range of motion and stability (Veeger & Van der Helm, 2007). Instability may be described as increased joint laxity or the loss of shoulder function and/or comfort due to increased translation of the humerus in the glenoid fossa (Lippitt et al, 1991). In modeling terms, the glenohumeral joint can be described as unstable when the glenohumeral joint reaction force does not intersect with the glenoid surface. This can be further qualified as any time the compression component of the joint reaction force is less than the resultant shear component of the glenohumeral joint reaction force. In general, the major stabilizing structures of the joint are the glenoid labrum, glenohumeral ligaments, the rotator cuff tendons, and the dynamic stabilization from the surrounding muscles themselves (Itoi et al, 1996; Kronberg et al, 1990). The labrum has been measured to contribute 50% more depth to the socket than the fossa alone (Howell et al, 1989). The translational force needed to dislocate a shoulder with an excised labrum is approximately 20% less than with an intact labrum in any direction and can reach 37% in the inferior and posteroinferior directions (Lippitt et al, 1993).

Lippitt and Matsen (1993) described two mechanisms of GH stability based on *in vitro* studies, "concavity-compression" and scapulohumeral balance. Concavity-compression is associated with the depth and width of the glenoid fossa, along with the magnitude of the compression force applied by the surrounding musculature. The study found these factors to have significant effects on the force needed to translate the head of the humerus in the glenoid fossa in 8 directions using cadavers (Figure 1). It was found that deeper fossa with higher compression forces were able to resist higher translational (shear) forces applied at the GH joint.

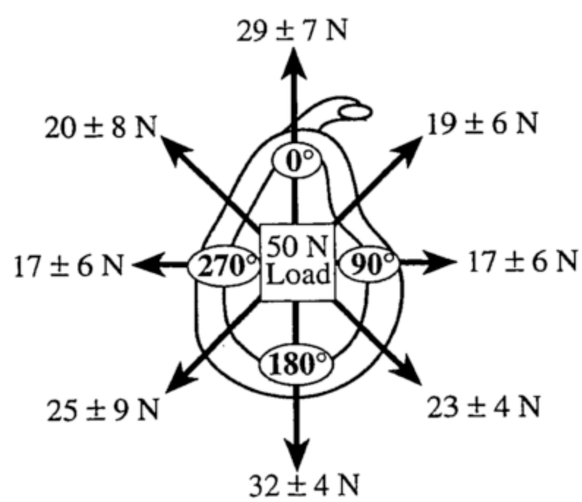

Figure 1. Average maximum translating force resisted in 8 directions (0°= superior, 90°= anterior) with a humeral head compression into the glenoid concavity of 50 N (Lippitt & Matsen, 1993).

Scapulohumeral balance refers to the joint reaction force of the GH joint being balanced within the surface of the glenoid fossa. Instability is said to occur when the net joint reaction force is not directed to intersect with the glenoid surface, instead it falls outside of the glenoid fossa causing the capsuloligamentous structures to tighten (Figure 2). It has been theorized that the rotator cuff muscles activate at different levels of force as needed to keep the joint reaction forces within the fossa (Lippitt & Matsen, 1993; Yanagawa et al, 2008).

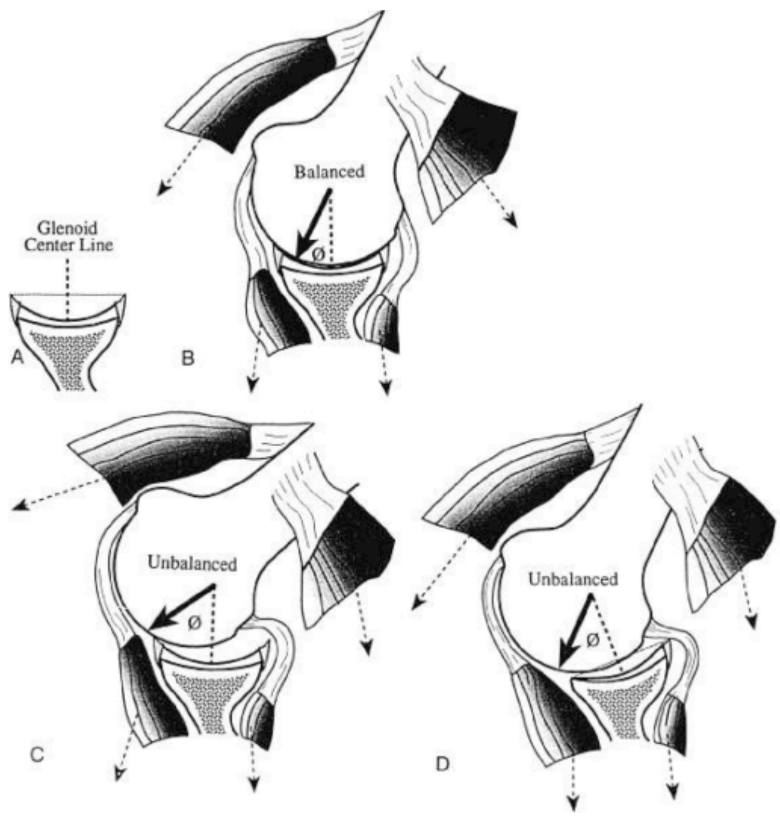

Figure 2. Overhead view of glenoid fossa and humerus. A) Glenoid centre is perpendicular to the midpoint of the glenoid concavity in an axis. B) Stable joint. C) Unstable joint since the joint reaction force is not directed into the cavity. D) Unstable joint due to abnormal glenoid version (Lippitt & Matsen, 1993).

The superior, middle, and inferior glenohumeral ligaments respectively prevent inferior/anterior translation, lateral rotation and anterior translation, and inferior/anterior translation of the humeral head when the arm is elevated. The coracohumeral ligament also prevents anterior translation of the humeral head (Culham & Peat, 1993). The muscles of the rotator cuff (supraspinatus, infraspinatus, subscapularis, teres minor) are the main source of dynamic stabilization of the GH joint especially in the anteroposterior axis due to their lines of action (Lee et al, 2000).

Ackland and Pandy (2009) observed the lines of actions of 13 major muscles and muscle 'sub-regions' which cross the GH joint through cadaveric testing (and modeling for latissimus dorsi and pectoralis major muscles). The study computed average stability ratios for each muscle to demonstrate their potential contribution to GH joint stability (Figure 3). An anterior/posterior and superior/inferior stability ratio were created for each muscle sub region based on the average shear component of the muscles line of action divided by the average compression component. They characterized a stabilizing muscle as having a compressive force component that is greater than its shear force component (stabilizing ratio <1) at the joint as well as having a line of action more inclined towards the joint centre. Conversely, a destabilizing muscle has a shear force component greater than its compressive force component (ratio >1) and has a line of action more inclined away from the joint centre. Both of these characterizations are situational based and dependent on joint angles (Ackland & Pandy, 2009). They demonstrated that the pectoralis major, and inferior latissimus dorsi sub regions have the most significant potential to cause a destabilizing shear force during abduction and flexion movements. They also described that most of the dynamic joint stabilization is from the rotator cuff muscles.

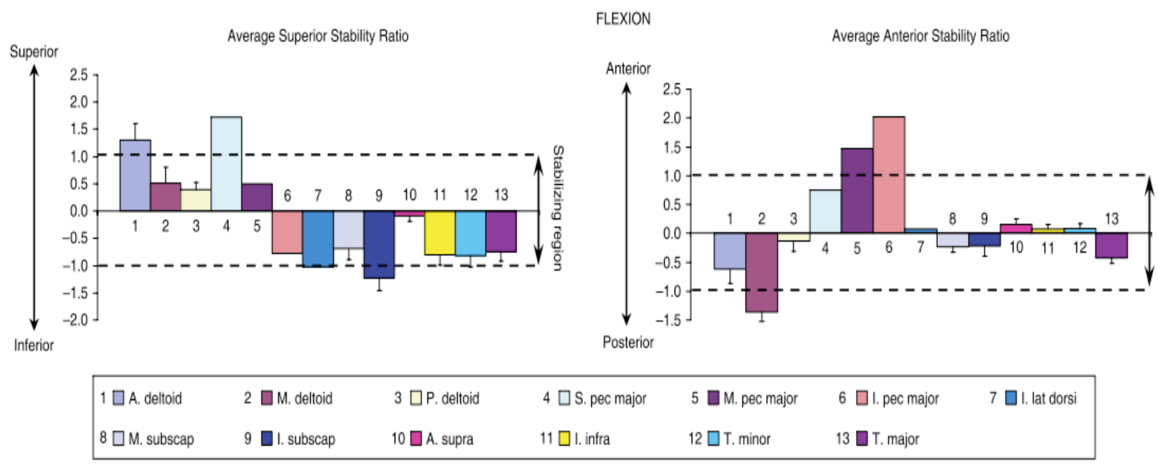

Figure 3. Average stability ratios for 13 shoulder muscles and muscle sub regions during arm flexion. Ratios between 1 & -1 are deemed stable (Ackland & Pandy, 2009).

In summary, the shoulder joint is not as stable as other joints in the body but is similar in that compressive forces stabilize the joint, shear forces destabilize the joint, and if the shear forces have a large enough magnitude a dislocation can occur. The labrum, joint capsule and ligaments act as passive stabilizers and surrounding muscles act as active stabilizers to reduce destabilizing shear forces. Active muscle stabilization has been shown to occur in the middle range of motion when ligaments are lax, while static capsuloligamentous stabilization tends to occur at the end range of motion when ligaments are in tension (Lee et al, 2000; Kronberg et al, 1990). Muscular fatigue has the potential to reduce the force output and muscle proprioception of the rotator cuff and, in turn, decrease dynamic stabilization, thereby increasing the risk for instability and injury in the shoulder (Morrison et al, 2000; Carpenter et al, 1998).

2.2 Incidence and Risk of Workplace Shoulder Injuries

By observing the anatomy of the shoulder, it is easy to see there are multiple possibilities for injury (muscle and ligament tears, dislocation, and impingement), but not as easy to see the underlying mechanisms for injury, such as impingement of the humerus against the acromioclavicular arch which can lead to an unstable shoulder, and in turn increase the risk of injury. Approximately 6.2% of all allowed lost time claims in Ontario involved the shoulder, and nearly all were "high impact" claims (Figure 4, WSIB, 2013). These claims are associated with slower recovery times, slower return to work times, and higher costs ($33,000 to $ 52,000) when compared to a regular lost time claim ($30,000) (WSIB, 2011). There are a few different events reported as causing shoulder injuries such as falls, and being struck by objects or equipment, but the highest recorded event was overexertion (WSIB, 2013). It is difficult to establish a simple causal relationship between overexertion and shoulder injuries, although some studies state that muscle fatigue can decrease dynamic stabilization of the shoulder joint (Bowman et al, 2006; Szucs et al, 2009; Carpenter et al, 1998). Shoulder instability can lead to inflammation and loosening of the joint capsule putting the worker at risk for impingement, muscle strains, and ligament sprains (Morrison et al, 2000; Yamamoto et al, 2010).

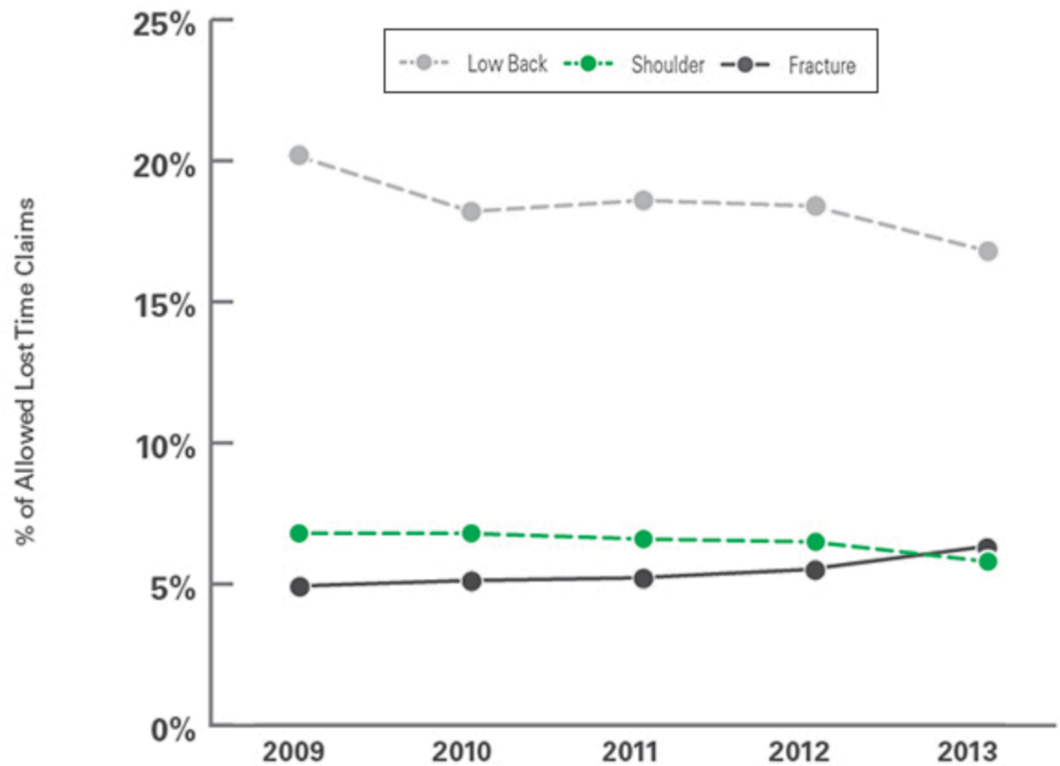

Figure 4. WSIB High Impact Claims during 2012, 6.3% of all claims were high impact shoulder claims (WSIB, 2013).

Svendson et al (2004) demonstrated an exposure-response relationship between elevated arm work and clinically verified shoulder disorders in 1800 Danish workers consisting mainly of painters and autoworkers. Frost et al (1999) also found a relationship between shoulder impingement and monotonous or intensive shoulder work in slaughterhouses. They found employees who worked with their arms above 30° of elevation for more than half of their total work time had a prevalence ratio of 5.27 (CI 2.09-13.26) for impingement syndrome, and previous employees demonstrated a prevalence ratio of 7.9 (CI 2.94-21.18), compared to workers at a nearby chemical plant where elevated arm work was minimal.

To help worker safety and reduce costly compensation claims, the incidence of shoulder injuries occurring in the workplace needs to be reduced. To reduce the incidence of injuries, the use of proactive ergonomics tools and models have become more prevalent (Chaffin, 2005). The use of proactive musculoskeletal models allow ergonomists to estimate safe working intensities and have been used to predict individual muscle activations during specific tasks (Laursen et al, 2003). With accurate proactive tools, such as biomechanical models, employees can work at a safe level of activity therefore reducing the number of injury claims.

2.3 Biomechanical Shoulder Models

Biomechanical models attempt to simulate the human anatomy and its function to predict outputs such as joint reaction and individual muscle forces which cannot be easily measured *in vivo* (Erdemir et al, 2007). Shoulder models have increased in complexity over the years, the first models developed by Mollier (1899), Shiino (1913), and Hvorslev (1927) used physical analogs similar to Figure 5. The models keys could be moved to change muscle lengths and move the model similar to a forward dynamic model. Conversely, moving the bones would change the key positions which could be related to muscle length changes essentially giving crude kinematics.

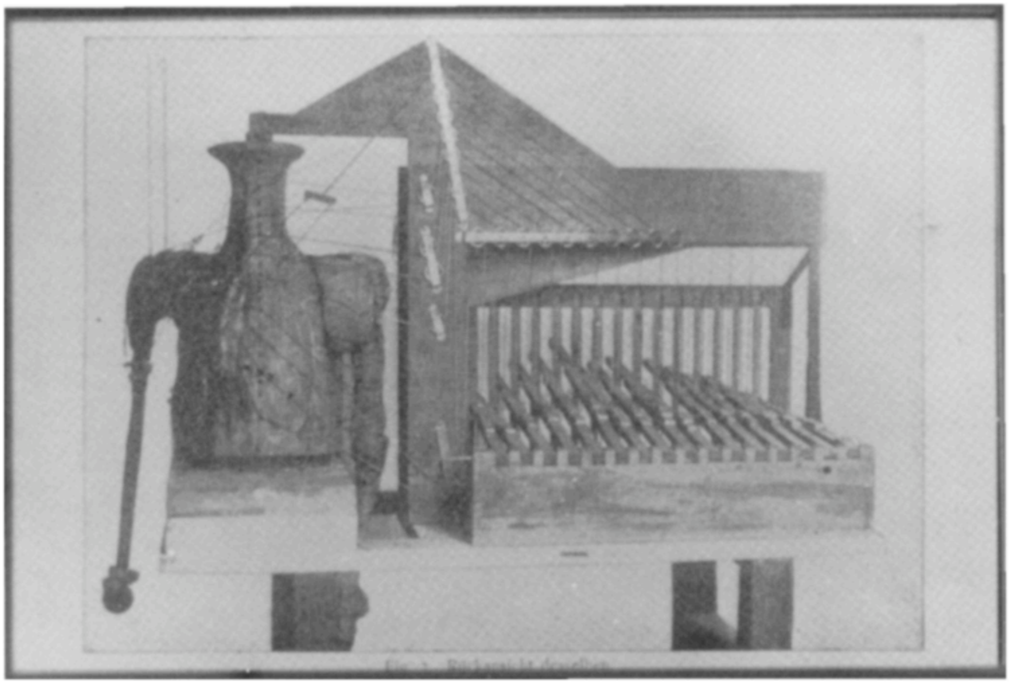

Figure 5. Mollier's 1899 Shoulder Muscle Model (from Van Der Helm, 1994a).

Over half a century later, two-dimensional models used instantaneous joint centres and muscle thickness from x-ray imagery to solve for the force of a particular shoulder muscle during an isometric contraction (De Luca & Forrest, 1973). Dul et al (1988) used a two dimensional model to predict individual muscle forces and muscle endurance at the shoulder. Over the past few decades, numerous three-dimensional models of the shoulder have been created and used for applications including biomechanics, ergonomics, rehabilitation, and orthopedics (Högfors et al, 1987; Karlsson and Peterson, 1992; Van der Helm, 1994a; Holzbaur, 2005; Dickerson et al, 2007). Högfors et al (1987) treated the shoulder as a 12-degree of freedom (DoF) system with 3 rigid bodies (clavicle, scapula, and humerus). Karlsson and Peterson (1992) further developed the Högfors et al (1987) model, introducing new constraints and also adding an optimization function which minimized the sum of squared muscle stresses. This function is based on the muscle force-endurance relationship and aimed to minimize muscle fatigue (Crowninshield & Brand, 1981). Holzbaur et al (2005) created a more inclusive model of the upper extremity including the shoulder, elbow, forearm, wrist, index finger, and thumb. The model includes 15 DoF with only 3 DoF at the shoulder (elevation plane, elevation angle, humeral rotation). Using the program SIMM (Software for Interactive Musculoskeletal Modeling, Musculographics Inc, Motion Analysis Corporation, Santa Rosa, CA), the model also implemented a non-linear static optimization to reduce muscle activation by promoting load sharing between muscles. Dickerson et al (2007) created one of the most recent shoulder models and introduced a novel shear constraint that uses an anisotropic glenohumeral stability index which quantitatively describes the non-dislocation conditions of the glenohumeral joint based on the cadaveric testing of Lippitt and Matsen (1993). Basically, the constraint forms a maximum force ratio for 8 different directions (Figure 6) that the glenohumeral contact force cannot exceed thus making the joint unable to dislocate. The threshold which determines the maximum is described by a ratio coefficient multiplied by the shear to compressive force ratio in the corresponding plane as seen in Figure 6.

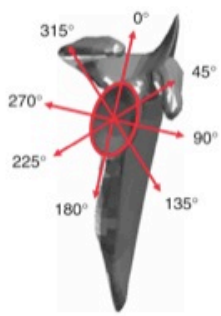

c_i

Direction	Dislocation Force Ratio Threshold (Shear/Compression) (%)
0	51
45	33
90	29
135	40
180	56
225	43
270	30
315	35

$$\boxed{J_{gh} = \sum_{i=1}^{8} c_i S_i \quad \text{given that : } \quad c_i \geq 0}$$

$$S_i = \frac{F_{s,i}}{F_c}$$

Shear Force

Compressive Force

Figure 6. Glenohumeral stability constraint, c_i = the ratio coefficient in the i^{th} direction, $F_{s,i}$= shear force acting in the i^{th} direction, F_c= compressive force directed into glenoid cavity (adapted from Dickerson et al, 2007).

The Delft Shoulder and Elbow Model (DSEM) proposed by Van der Helm (1994a) has been one of the most visible in the literature. It has been used for applications such as studying tendon transfers (Magermans et al, 2004), shoulder stability based on rotator cuff tears (Steenbrink et al, 2009), and wheel chair propulsion (Veeger et al, 2002). The DSEM is a finite element model produced using a software program SPACAR based on non-linear finite elements for multi-degree of freedom mechanisms (Dept. Engineering Mechanics, Delft University of Technology). The model uses elements of simple shapes and different properties to represent morphological structures of the shoulder (Figure 7). Beam (bone), active truss (muscle), passive truss (ligament) and hinge (joint) elements were used to model muscle stresses and forces based on kinematics. Special elements such as curved trusses and "surface" elements were used for muscle wrapping and constraining the medial border of the scapula to the thorax respectively. The special elements were used to better replicate the complex shoulder anatomy (Van der Helm, 1994a). The DSEM, which was built in SIMM by Blana et al

(2008), consists of 29 muscles represented by 138 muscle elements. The number of muscle elements which represent a specific muscle is based on the muscles size and width. For example, the pectoralis major sternal head is larger and wider than the clavicular head therefore there are 6 muscle elements for the sternal head and only 2 for the clavicular head. The model uses the same anatomical dataset (Klein-Breteler et al, 1999), and optimization criterion (sum of squared or cubed muscle stresses), as the finite element DSEM but uses more recent SIMM algorithms for muscle wrapping rather than the SPACAR algorithms used in the original DSEM model.

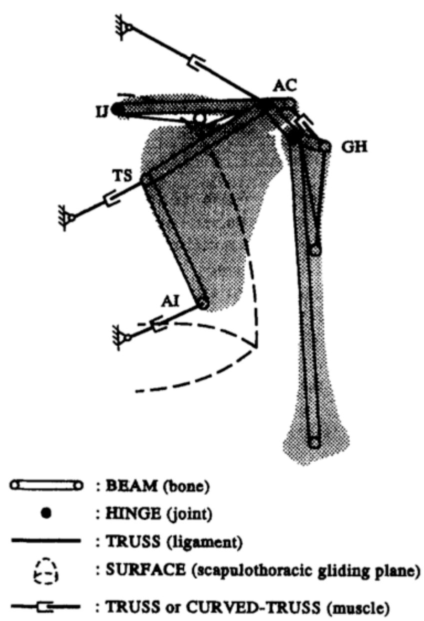

Figure 7. DSM Finite Element Model Right Shoulder Complex (not all muscles and ligaments shown)(Van der Helm 1994a)

The DSEM model in OpenSIM uses the muscle parameters and geometry described in Klein-Breteler et al (1999) for the shoulder and (Minekus, 1997) for the elbow. Both studies used the same 57 year old male specimen and recorded the number of sarcomeres for each muscle (using laser diffraction technique), optimal muscle fibre length, tendon length, and physiological cross sectional area (PCSA). The studies also digitized the joint surfaces and bone shapes to model geometrical forms, as well as collected the position of bony landmarks and contours for muscle wrapping. Joint angles (kinematic data), and external forces are used as input for the model to output predicted muscle activations, forces and joint reaction forces.

To calculate joint angles in OpenSIM the inverse kinematic (IK) tool takes marker position data as well as joint angles as input, and outputs an angle for each degree of freedom in the model (joint angles) for every frame based on a weighted least squares function (Equation 1). The DSEM model implemented in OpenSIM has 11 degrees of freedom, 3 at the sternoclavicular joint, 3 at the acromioclavicular joint, 3 at the glenohumeral joint, 1 at the elbow, and 1 at the forearm.

$$J = \underset{q}{min}\left[\sum_{i \in markers} w_i \left\| x_i^{exp} - x_i(q) \right\| + \sum_{j \in \text{unprescribed angles}} w_j \left(q_j^{exp} - q_j\right)^2\right] \qquad (1)$$

$$* \ q_i = q_i^{exp} \text{ for all prescribed angles j}$$

where, q is the vector of generalized joint angles being solved for, x_i^{exp} is the experimental position of marker i, $x_i(q)$ is the position of the corresponding marker in the model, q_j^{exp} is the experimental value for joint angle j, and prescribed angles are those that have a value inputted (for example the elbow would have a prescribed angle of 90° if it was locked for the duration of the motion at 90°).

This equation aims to minimize the marker error and the joint angle error. Marker error is described as the distance between the experimental marker and the corresponding marker on the model. Joint angle error is the difference between the experimental joint angle and the angle computed by the IK tool. Marker weights (w_i) are selected by the user to specify how strongly a markers error is minimized, in other words a marker with a higher weight relative to others will be tracked better than other markers during IK. Similarly, joint angle weights (w_j) are selected to specify how strongly a single joint angles error is minimized relative to others if the angle has not already been prescribed.

Once a motion is prescribed, a set of joint angles from the IK tool in OpenSIM uses the motion and any external forces applied to the body to calculate net joint moments acting at each degree of freedom. The static optimization tool further resolves the net joint moments into individual muscle forces based on the solution of an optimization function for each frame in the motion.

The original DSEM model has two possible optimization criteria: 1) a stress cost optimization (Equation 2), which minimizes the sum of the cubed muscle stresses (Crowninshield & Brand, 1981), and 2) a metabolic cost optimization, which minimizes the metabolic cost attributed to muscle physiological processes (crossbridge formation and calcium pumps) during the motion (Praagman et al, 2006). The DSEM implemented in OpenSIM uses a static optimization criterion (Equation 3), which minimizes muscle activations to a designated power (x) (Anderson & Pandy, 2001). Recently, a plugin was created by Macintosh (2014) which enables the use of the entropy-assisted optimization model (Equation 4) created by (Jiang and Mirka, 2007).

Sum of Muscle Stresses $$J = \sum_{i=1}^{n} \left(\frac{F_i}{PCSA_i} \right)^3 \qquad (2)$$

Where F_i is the individual muscle force, and $PCSA_i$ is the physiological crosssectional area. (Crowninshield & Brand, 1981)

Sum of Muscle Activations $$J = \sum_{i=1}^{n} (a_i)^x \qquad (3)$$

Where a_i is the individual muscle activation, and x is a number (usually 2 or 3) (Anderson & Pandy, 2001)

Entropy-Assisted $$J = (1 - W) \sum_{i=1}^{n} (a_i)^x + W \sum_{i=1}^{n} a_i \, log a_i \qquad (4)$$

Where W is a weight factor expressing how strongly the sum of muscle activations or entropy term is used, a_i is the individual muscle activation, and x is a number. (Jiang & Mirka, 2007)

All three of the above equations can be used to solve the muscle redundacy problem but will yield different solutions. Pedotti et al (1978) found the sum of muscle forces squared to yeild results closer to EMG than a linear equation and Crowninshield & Brant (1981) found a cubic function produced better results than a squared function for the sum of muscle stresses. They also noted that using a power of 2, 3, or 4 did not change the number of predicted muscles but did change the predicted values for individual muscle forces. The cubed function is associated with the maximization of muscle endurance and promotes agonist activity from muscles with a larger moment arm and crosssectional area. In order to predict co-contraction, Jiang and Mirka (2007) introduced an entropy-assisted optimization criterion which is based on the weighted sum of two systems. The first favours agonist muscle activation and the second, described by the entropy term, favours agonist-antagonist co-contraction. Jiang and Mirka (2007) tested this optimization using an elbow flexion task and reported an average r^2 of 0.48 for elbow flexors, and 0.46 for elbow extensors, when comparing the predicted and experimental muscle forces.

In order to quantify and compare the measure of co-contraction between two muscles with different levels of EMG activation (EMG_{High} and EMG_{Low}), a concontraction index (CCI) is necessary. The CCI (Equation 5) provides a means of quantification of co-activation between a muscle pair over a specified period of time (Lewek et al, 2004; Holmes & Keir, 2012).

$$CCI = \sum_{i=1}^{N}\left[\left(\frac{EMG_{low\,(i)}}{EMG_{high\,(i)}}\right)\left(EMG_{low\,(i)} + EMG_{high\,(i)}\right)\right] \qquad (5)$$

Models use optimization functions and constraints to help produce output. Constraints are used to restrict muscle models in a way that allows faster and better model performance, sometimes giving up anatomical fidelity in the process. The DSEM has some major constraints, the trigonum spinae and angulus inferior elements of the scapula are constrained to a specific distance from the thorax to create the scapulothoracic gliding plane, and another constraint limits the glenohumeral joint reaction force (JRF) to intersecting the surface of the glenoid. Karlsson and Peterson (1992) did not include a glenohumeral JRF constraint but stated a need for constraint of its direction. Dickerson et al (2007) implemented a unique constraint, which used directional dislocation thresholds as limits for the JRF. By constraining the JRF similar to Dickerson et al (2007) or the DSEM, the humerus is mathematically unable to dislocate from the glenoid (shear/compression ratio cannot exceed set threshold), this makes the model more stable but also less anatomically and functionally correct. Steenbrink et al (2009) simulated different rotator cuff muscle tears using the DSEM with and without the stability constraint for a static position at approximately 80° of arm elevation. With only the supraspinatus muscle removed both the constraint and non constraint models performed fairly similar, but once another muscle was removed (such as infraspinatus in Figure 8) the constrained and non constrained models begin to act differently. With less stability from muscles, the constrained model increases the force from teres minor and subscapularis to maintain the glenohumeral JRF within the glenoid, where as the unconstrained model allows the humerus to dislocate. There is evidence based on the lines of action and EMG activation that the rotator cuff muscles do stabilize the shoulder (Kronberg et al, 1990; Lippitt & Matsen, 1993; Yanagawa et al, 2008; Ackland & Pandy, 2009), but with enough shear force even the strongest muscles will allow shoulder dislocations which is not replicated in a model with a glenohumeral JRF constraint.

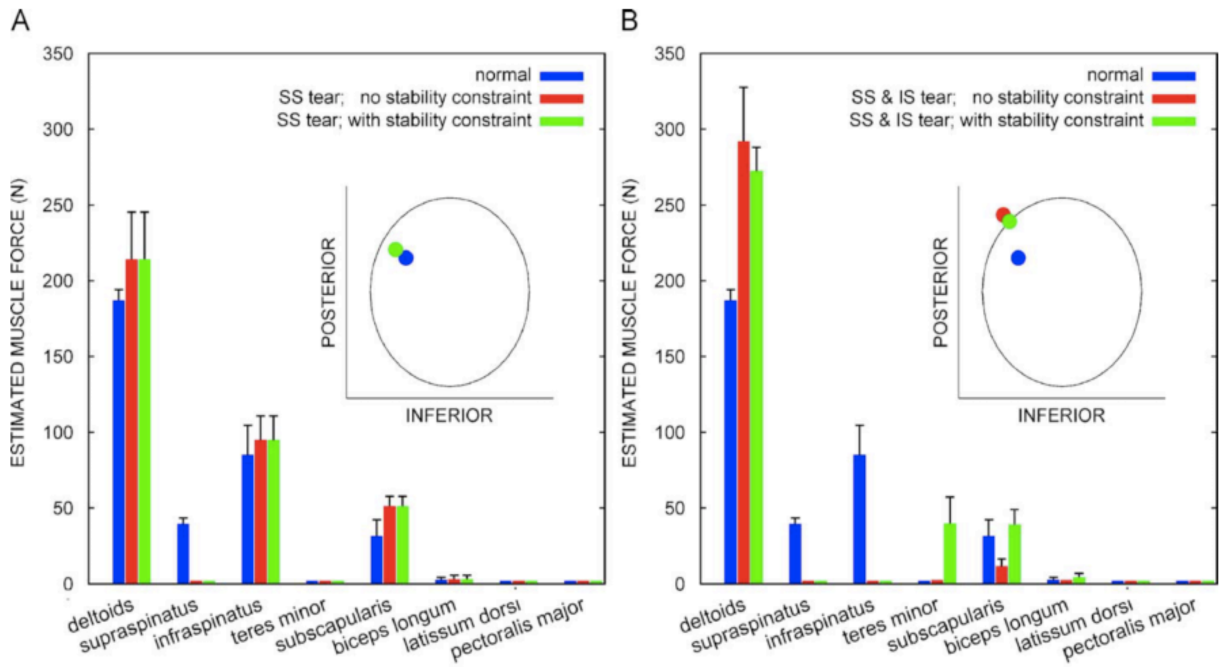

Figure 8. Estimated muscle forces (chart) and glenohumeral JRF position within glenoid (circle) during a supraspinatus tear (A) and a supraspinatus and infraspinatus tear (B) for constrained and unconstrained conditions (Steenbrink et al, 2009).

2.4 Model Validation Techniques

Validity is a concern with any musculoskeletal model. Due to the feasibility of measuring muscle forces *in vivo* to compare to model predicted forces, indirect methods are used. Indirect methods involve correlating recorded EMG to the model's predicted force (Van der Helm, 1994b; De Groot et al, 2004; Nikooyan et al, 2011). The DSEM model has been validated qualitatively and attempts have been made to validate it quantitatively. Van der Helm (1994b) used kinematic data (bony landmark coordinates were found using a spatial digitizer) from shoulder abduction and flexion movements under loaded (750 gram weight in hand) and unloaded conditions, as input to predict shoulder muscle forces with the inverse dynamics Delft Shoulder Model. EMG from 12 shoulder muscles was collected simultaneously with the kinematic data. The on/off patterns for the muscles were qualitatively compared to the model's predicted force data during the movements. Over a decade later, Nikooyan et al (2011) compared 12 shoulder muscles and the DSEM to predict force-time series during a slow shoulder flexion task. A relatively good relationship was found based on cross correlations between model predicted normalized muscle force-time series and normalized EMG (average of all 12 muscles R~0.71), but data were only collected on one subject whom had a shoulder hemi-arthroplasty. Blana et al (2008) collected EMG and kinematic data while participants performed shoulder movements in multiple planes as well as elbow movements and activities of daily living. Similar to Van Der Helm (1994) and Nikooyan et al (2011), Blana et al (2008) compared the signal shape and timing with the muscle model's force-time curves in order to validate their shoulder model. Cross correlation values for each muscle were averaged across all tasks and varied depending on the muscle (0.29 - 0.75, mean correlation = 0.46). The highest correlations were seen in the deltoids, and lowest in the biceps and triceps. Other studies have used the mean absolute error (MAE) to indirectly, but quantitatively, validate upper extremity musculoskeletal models (Dubowsky et al, 2008, Morrow et al, 2010) although RMSE (root mean square error), as seen in Nikooyan et al. (2013) and Liu et al (1999), may be more applicable since it weights larger errors higher.

2.5. Purpose

1) To compare the performance of several optimization functions (models), using the DSEM implemented in OpenSIM, with experimental EMG recordings.

2) To evaluate the ability of each model to predict co-contraction for several postures and actions.

3) To evaluate estimated joint reaction forces and joint translational stability (shear/compression force ratio) at the glenohumeral joint in multiple postures.

2.6. Hypotheses

1) Based on the literature, it was predicted that the cubic optimization function, minimizing activation, would have the lowest RMSE and highest correlation when compared to experimental EMG.

2) The entropy model would predict significantly higher CCI than all other optimization functions, and the apprehension position would elicit the highest CCI of all positions.

3) The joint will be most stable using the entropy model, due to the possibility of increased co-contraction. It was also predicted that the glenohumeral joint reaction shear force would be the largest in all models for the apprehension posture.

3. METHODS

3.1. Data Acquisition

3.1.1 Participants

Ten healthy right hand dominant male participants, free of any upper extremity disorders, trauma, and or shoulder pain within the past 12 months, were recruited from the university community. All participants provided informed written consent prior to data collection and the study was approved by the McMaster University Research Ethics Board.

3.1.2. Collection Protocol

Data collection consisted of a series of static and dynamic tasks as well as a glenohumeral stress test. All tasks were performed, as arm elevation or rotation movements, in a seated position using an isokinetic dynamometer. In addition to the torque from the dynamometer, EMG, and motion capture were recorded. Static tasks were performed as a ramp contraction over two seconds, then held for three seconds before ramping down. These were performed at 60° and 120° of arm elevation in the flexion plane. At each position, flexion exertions were recorded at high (35 Nm) and low (10 Nm) torque levels under high and low shear conditions (Figure 9). This resulted in a total of eight static trials. The shear conditions were manipulated with two different points of force application, relative to the GH joint (distal forearm, and upper arm), to produce different shear forces at the glenohumeral joint while keeping the moment arms of the muscle's constant. This was necessary for later comparisons, since muscle moment arms have been shown to be a sensitive parameter in muscle force prediction (Raikova & Prilutsky 2001).

The dynamic trials were performed as arm elevation movements, in the three planes illustrated in Figure 9, using the same two points of force application as the static trials. Each trial was performed as 3 consecutive arm elevation movements over a range of motion from 0° to 135°, with a straight arm and the humerus in a neutral posture (no internal or external rotation). Using the Biodex in isotonic mode, each velocity was performed at a high and low level of torque (35 Nm and 10 Nm respectively). These torque levels were approximately 60% and 10% of healthy male maximum isokinetic torque performed at 60°/sec (Cahalan et al, 1991; Danneskiold-Samsøe et al, 2009).

A subset of dynamic trials were repeated while sitting in the same apparatus, but moving the arm freely without the use of the dynamometer, to test whether the dynamometer constrains shoulder movement. The trials consisted of arm elevations in the sagittal plane at 60°/sec and 120°/sec without a weight similar to actions analyzed by Van Der Helm (1994b).

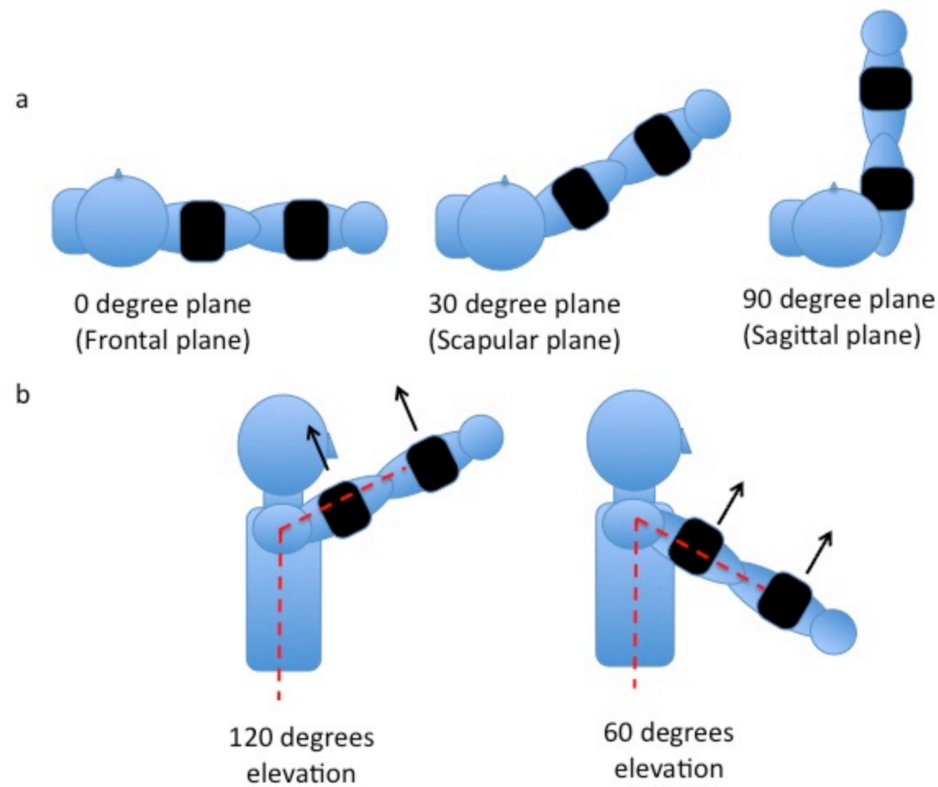

Figure 9. Postures for protocol, a; top down view of three different planes of action. b; 2 different elevation angles. Black straps and arrows designate positions and approximate direction of the force application.

The final trial was a glenohumeral stress test performed in the 'apprehension position' (Figure 10). This position puts the shoulder in an unstable position by increasing shear forces at the GH joint (Labriola et al, 2005). The apprehension position approximates 90° of abduction and 90° external rotation of the humerus with 90° of elbow flexion (Lo et al, 2004). This position places an anterior and slightly inferior shear force on the humeral head, which may increase the shear components (mainly anterior/posterior component) of the glenohumeral joint reaction force seen in the model. This trial was performed in a seated position similar to the static and dynamic trials but the participant was asked to externally rotate their humerus (push backwards) against the Biodex attachment using a ramp contraction of approximately 75% of the subject's maximum strength, or as much as they felt comfortable with. All static, dynamic, and stress test trials have been summarized in Table 1.

Figure 10. Glenohumeral stress test (apprehension position).

Table 1: Summary of trials.

Condition Type	Plane of action	Shear Positions	Force Levels	# of Angles	# of Speeds	Exertion Type	**Total**
Static	1	2	2	2	1	Flexion	**8**
Dynamic with Biodex	3	2	2	---	2	Flexion	**24**
Dynamic w/o Biodex	1	1	1	---	2	Flexion	**2**
Glenohumeral Stress Test	1	1	1	1	1	Ext. Rotation	**1**

All trials were block randomized and separated by at least 2 minutes of rest to reduce the effect of fatigue. Torque was displayed on a monitor located in front of the subject, for static trials, to enable real-time feedback. A gold line spanning across a chart designated the target torque and a red line designated the real-time torque value. Movement velocity was set at 60°/sec and 120°/sec for dynamic trials. Velocity of motion was controlled using a visual and audible aid presented on the monitor (Figure 11). The animation was played on a loop and the subject would watch it for a few cycles before starting the movement when they were ready.

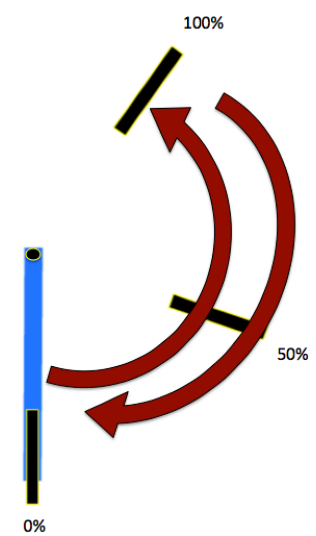

Figure 11. Snapshot of visual feedback animation on monitor during dynamic trials. The blue bar (arm) would rotate back and forth through the described range of motion (annotated by red arrows) to mimic flexion and extension. Metronome tones were audible when the blue bar passed a black line representing either 0%, 50%, or 100% completion of the prescribed range of the motion.

EMG signals were normalized to a maximum voluntary dynamic concentric contraction (MVDC) obtained from each muscle before the collection protocol, using the equipment outlined in the section 3.1.3. Hodder & Keir (2013) demonstrated MVDC's elicit higher muscle activity than isometric trials in most subjects, for all of the muscles being collected in the present study (Table 2) except for latissimus dorsi (isometric contractions elicited the highest MVC in most participants) and supraspinatus (supraspinatus was not included in the study). Maximum abduction-adduction, flexion-extension, and internal-external rotations of the shoulder were performed on the Biodex to record MVDC's for all muscles in addition to manually resisted MVC's (Table 2). Abduction-adduction was performed from 0°-135° with a straight arm, flexion-extension was performed from 0°-135° with a straight arm, and internal-external rotation was performed from 0° of rotation to the participants maximum external rotation (approximately 75°) with the arm abducted 45° and elbow flexed to 90°. All of the MVDC's were performed at 30°/sec as this has been seen to elicit the highest muscle activation (Hodder & Keir, 2013). In the event higher muscle activation was reached during a collection trial, it was used for normalization.

Table 2: Summary of actions used to elicit isometric and dynamic MVC's in recorded muscles.

Muscle	MVC Manually Resisted Action	MVDC Action Using Biodex
Anterior Deltoid	Forward flexion of arm resisted at 60° of flexion	Flexion
Middle Deltoid	Abduction of arm resisted at 60° of abduction	Abduction
Posterior Deltoid	Horizontal cross extension of arm resisted at 90° of abduction	Extension
Pectoralis Major (Sternocostal head)	Internal rotation with slight adduction of arm resisted when arm was abducted to 90° and elbow flexed to 90°	Internal Rotation or Flexion
Supraspinatus	Abduction of arm resisted at 0° of abduction (arm at side)	Abduction
Infraspinatus	External rotation resisted when arm is at 0° of abduction and elbow is at 90° of flexion	External Rotation
Latissimus Dorsi	Adduction resisted when arm is abducted at 90° and elbow is flexed to 90°	Adduction
Trapezius Upper Fibres	Participant was asked to grab underneath Biodex chair and shrug shoulder	Abduction or Flexion

3.1.3. Apparatus and Instruments

An isokinetic dynamometer (Biodex System 4, Biodex Medical Systems, NY) was customized to have the participant secured in a seated position while enabling full range of motion at the shoulder complex (Figure 12). A custom foam spacer was used to ensure clearance of EMG electrodes and motion capture markers between the participant's scapula, shoulder, and humerus and the back rest of the Biodex chair. The participant was seated with a torso strap to reduce the amount of leaning and unwanted muscle activation from the lower back musculature. The participant's arm lifted against a firm pad attached to the Biodex. The attachment was adjustable in length for the two points of force application.

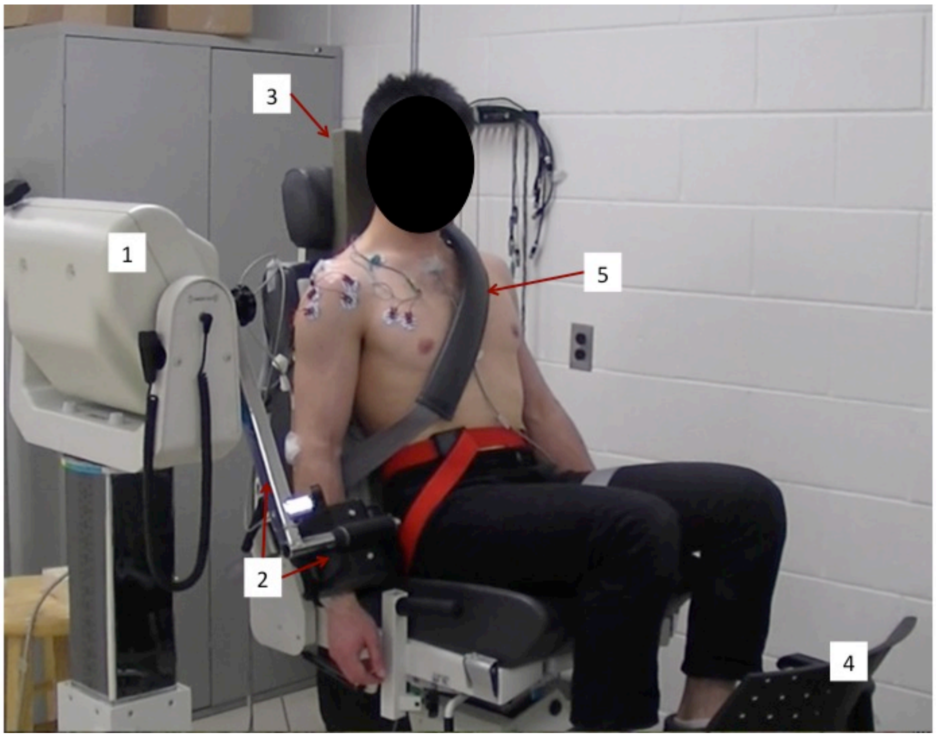

Figure 12. Biodex setup with pad attachment during sagittal plane flexion movement. 1) Biodex System 4 dynamometer, 2) custom arm attachment and pad, 3) custom foam spacer, 4) foot rest, 5) torso strap.

The isokinetic dynamometer was used to collect joint torque and angle data at 100 Hz for all trials (except trials without the Biodex). Data were filtered using an analog 1st order low pass filter (f_c =200 Hz) before being digitized. The measured torque and moment arm (length from acromion to force application) were used to calculate force after the torque data were gravity corrected. The calculated force was used for input as an external force in the shoulder model. The torque data were gravity corrected post collection using Equation 6:

$$T_{final} = \left[sin\left(\theta_{position}\right) * T_{Limb\ Weight}\right] + T_{Biodex\ Output} \quad (6)$$

Where T_{final} is the gravity corrected torque in Nm, θ is the position of the arm in degrees, $T_{Limb\ Weight}$ is the torque of the arm weight recorded at 90° of flexion, and $T_{Biodex\ Output}$ is the measured torque before gravity correction. The correction is always added to the $T_{Biodex\ Output}$ since only flexion and abduction movements were processed, if the movement was extension or adduction, the correction must be subtracted from $T_{Biodex\ Output}$.

Kinematic data were recorded using an electromagnetic tracking device, (Polhemus Fastrak, Colchester, VT, USA) with 4 electromagnetic sensors. The sensors report coordinate (x,y,z) and attitude data (azimuth, elevation, and roll) based on sensor position and orientation relative to the transmitter. Kinematic data were sampled at the system maximum of 30 Hz/sensor. The system was calibrated as described in the manual (FASTRAK Users Manual, 2002) before use to ensure the sensors were recording properly in degrees as well as centimeters. Sensors were placed on the incisura jugularis (DSEM model origin), the most lateral and posterior portion of the acromion, between the medial and lateral epicondyles on the posterior aspect of the humerus, and between the styloid processes on the posterior aspect of the forearm similar to other upper extremity kinematic studies (McQuade & Smidt, 1998; Ludewig & Cook, 2000; McClure et al, 2001). A custom scapula attachment for the acromion sensor based on Karduna et al (2001) was not used as it interfered with infraspinatus and supraspinatus EMG placement as well as had a higher likelihood of colliding with the back of the Biodex chair and causing unwanted motion of the sensor during movements.

EMG was recorded to be compared with the predicted muscle activation from the model. As there are more muscles in the model than can be feasibly collected (29 muscles in the model), 8 were recorded using EMG. The muscles were chosen based on their location and function in regards to the humerus and GH joint. The infraspinatus, supraspinatus, teres minor, and subscapularis muscles have been described as the main stabilizers of the GH joint (Itoi et al, 1996; Lee et al, 2000) but only the infraspinatus and supraspinatus was collected, as these muscles have been previously collected using surface EMG techniques (Kisiel-Sajewicz et al, 2011; Allen et al, 2013) where teres minor and subscapularis would need indwelling EMG in order to record muscle activity (Waite et al, 2010). The pectoralis major, anterior deltoid, middle deltoid, posterior deltoid, latissimus dorsi, trapezius upper fibres, and infraspinatus were recorded using disposable Ag/AgCl bipolar surface EMG electrodes. However, the supraspinatus was recorded using pediatric sized disposable Ag/AgCl bipolar surface EMG electrodes. Prior to surface EMG application, the skin was shaved as necessary and scrubbed with isopropyl alcohol swabs. Electrodes were then placed over the belly of the muscle parallel to the direction of muscle fibres. Proper electrode placement was confirmed by manually resisted test maneuvers which target the innervation of specific muscles (Table 3).

Table 3: Electrode placements and test maneuvers (adapted from Perotto et al, 2005).

Muscle	Electrode Placement	Posture	Test Maneuver
Anterior Deltoid	3 fingerbreadths below anterior margin of the acromion	Standing neutral posture	Forward elevation of the arm
Middle Deltoid	Halfway between the tip of the acromion and the deltoid tubercle	Standing neutral posture	Abduction of arm
Posterior Deltoid	2 fingerbreadths caudal to posterior margin of the acromion	Standing with arm abducted to 90° and elbow flexed	Horizontal arm extension in abducted position
Pectoralis Major	1 fingerbreadth medial to anterior axillary fold	Standing neutral posture	Horizontal adduction of arm
Supraspinatus	Just above the middle of the spine of the scapula	Prone with arm abducted 90° and elbow flexed	External rotation of humerus
Infraspinatus	2 fingerbreadths below medial portion of spine of scapula	Prone with arm abducted 90° and elbow flexed	External rotation of humerus
Latissimus Dorsi	3 fingerbreadths distal to and along the posterior axillary fold	Standing with arm abducted 90° externally rotated 90° and elbow flexed	Arm adduction
Trapezius Upper Fibres	At angle of neck and shoulder	Standing neutral posture	Shrug shoulder

A differential EMG amplifier (10-1000 Hz bandpass filter, input impedance=10 GOhms, CMRR=115 Db at 60 Hz, AMT-8, Bortec, Calgary, AB), and a 16 bit A/D converter (NI USB-6229,16 bit, 250 kS/s National Instruments, TX, USA) were used to collect data. Surface EMG was sampled at 2040 Hz. EMG, kinematics, torque, and position data were collected simultaneously using a program custom built with LabView Software (National Instruments, TX, USA).

3.2. Data Analysis

3.2.1. Kinematics and EMG processing

EMG of each muscle was de-biased, full wave rectified, and digitally filtered using a critically damped dual low pass filter (f_c = 4 Hz). Filtered EMG was normalized to the maximum activity found during the MVDC trials. The sensors coordinate and attitude data were low pass filtered using a critically damped dual low pass filter (f_c = 4 Hz). The kinematic, normalized EMG, and force data were cut into clips to isolate the flexion portion of each dynamic trial as well as to isolate the 3 seconds of constant contraction during static tasks. The coordinate data were converted from the Fastrak reference frame to the OpenSIM reference frame as well as converted to a local reference frame using the sternum marker as the origin. Virtual markers were added to the root of the spine (trigonum scapulae), as well as the inferior angle in order to approximate the scapula during inverse kinematics. These virtual markers were created relative to the acromion marker as per the scapular anthropometrics from Von Schroeder et al (2001) cadaveric study. All data were processed using a custom program (MATLAB R2012a, MathWorks, MA, USA).

The attitude data were used to create joint angles for forearm pronation/supination (PS_y), elbow flexion/extension (EL_x), and glenohumeral rotation/elevation/rotation (GH_y, GH_z, GH_yy) for input into OpenSIM (joint angle short forms in brackets). No sensors were placed on the clavicle, therefore, the 3 angles of the sternoclavicular joint (SC_y, SC_z, SC_x), as well as the 3 angles of the acromioclavicular joint (AC_y, AC_z, AC_x) expressed in the model, were not calculated from sensor data. An existing

MATLAB program (Charles, 2012) was adapted to take azimuth, elevation and roll data from Fastrak, as input, and perform inverse kinematics to calculate joint angles as output for OpenSIM. The joint angles were created using an Euler rotation sequence based on ISB recommendations. A sequence of Y-X-Y was used for the glenohumeral joint (section 2.4.4), Z-X-Y for the humeroulnar joint (section 3.4.2), and X-Y-Z for the radioulnar joint (section 3.4.3) (Wu et al, 2005).

3.2.2. Scaling, Inverse Kinematics, & Static Optimization

Marker files (.trc), joint angle files (.sto) and external force files (.sto) were created for every trial. OpenSIM tools were used to scale the model, produce a set of joint angles (IK tool), output predicted muscle activations and forces (static optimization), and output joint reaction forces based on the predicted muscle forces (see Figure 13 for process).

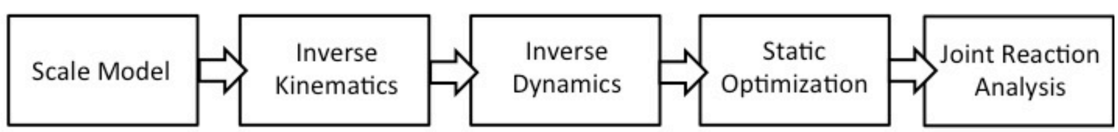

Figure 13. Schematic of the process of analysis in OpenSIM to obtain muscle and joint reaction forces.

The scale tool was used to take the generic DSEM model (Figure 14) and adjust the dimensions of the segments, as well as the inertial properties, to make the model subject specific. The body segments were scaled by adjusting the virtual marker set (attached to the generic model segments) to match the inputted experimental marker set for a static trial with the arm at 60°. The masses of the subject's torso, and upper limb were calculated based on the subjects mass in kilograms and Dempster's body segment parameters (Winter, 1990) to scale the mass of the segments and, in turn, scale the model's inertial parameters as well. An individual scaled model was produced for each of the ten subjects.

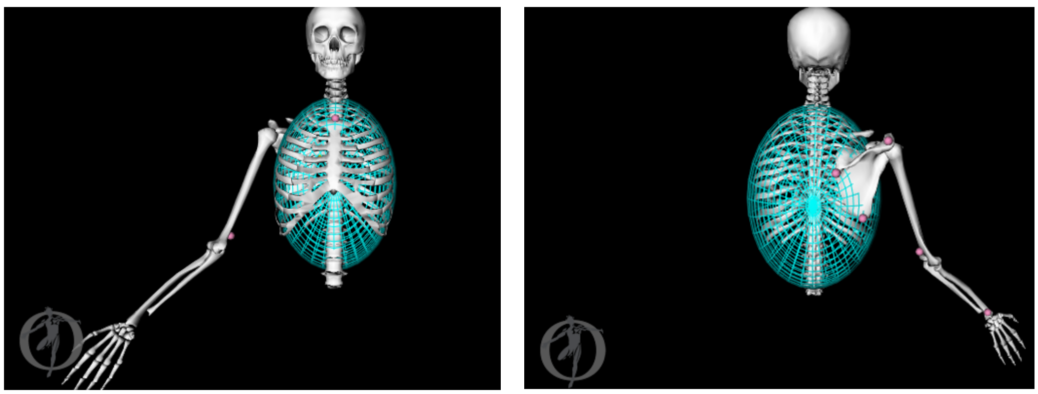

Figure 14. OpenSIM DSEM model with bones, virtual marker set (6 pink spheres), and thoracic wrap object (blue mesh).

The IK tool was used next to output a motion file of joint angles for all joints in the model, based on Equation 1, since the AC and SC joints were not calculated prior. The IK tool weights w_i and w_j were manually adjusted for each trial until a solution matched the experimental motion for the trial.

The motion from the IK tool, and the calculated force file from the recorded torque, were used by the inverse dynamics tool to output net joint moments. The force file was applied as a point force in the Z axis of the ulna or humerus, located 6.5 cm (length from marker to middle of pad) proximal to the forearm or humerus marker, depending on whether the pad was on the upper or lower arm for the trial. Since the force was calculated from torque, it was unidirectional, and assumed to be directed straight into the centre of the pad.

The static optimization tool was used immediately after inverse dynamics to solve for the combination of individual muscle activations that would produce the net joint moment found by the inverse dynamics tool, yet minimize a selected optimization function. The tool then outputted the predicted individual muscle activations and forces. Four optimization functions were used and are described as variations of equations 3 and 4. The sum of muscle activations (Equation 3) was used as a quadratic (x=2), cubed (x=3) and quartic function (x=4), and the entropy-assisted optimization (Equation 4) was used with an entropy weight factor (W) of 0.5, to split the contributions of the two terms equally (Jiang & Mirka, 2007). The outputted individual muscle forces were then used by the joint reaction analysis to predict joint reaction forces for the glenohumeral joint. More specifically, the force acting from the humerus on the scapula presented in the scapular reference frame (Figure 15).

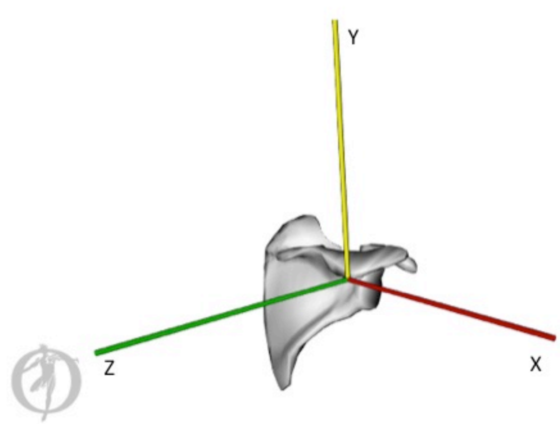

Figure 15. Scapular Reference Frame in OpenSIM. Z and Y joint reaction force components are shear, X joint reaction force component is compression.

The predicted and experimental muscle activities were compared using two methods. A cross correlation analysis was performed to reflect the similarity between the shapes of the muscle activation curves, and the root mean squared difference (RMSD) assessed differences in magnitude. RMSD was calculated as the difference between normalized predicted and experimental data and the cross correlation was expressed as the maximum explained variance (r^2) found between the predicted and experimental activation after the signals were phase shifted 20 frames in each direction.

3.2.3. Muscle Matching & Co-Contraction Index (CCI)

The DSEM represents each anatomical muscle with multiple muscle elements. The mean activation of multiple elements was used to represent the activation of a single muscle (Table 4). The mean predicted activation was then compared to the corresponding experimentally recorded muscle.

Table 4: Corresponding muscle elements for each recorded muscle.

Muscle	**Corresponding Muscle Elements from DSEM**
Anterior Deltoid	Delt_Clav 1,2,3,4
Middle Deltoid	Delt_Scap 5,6,7,8,9,10,11
Posterior Deltoid	Delt_Scap 1,2,3,4
Pectoralis Major (SC head)	Pect_Maj_T 1,2,3,4
Supraspinatus	Supra 1,2,3,4
Infraspinatus	Infra 1,2,3,4,5
Latissimus Dorsi	Lat_Dorsi 1,2,3,4,5,6
Trapezius Upper Fibres	Trap_Clav 1,2

The CCI (Equation 5) was calculated for several muscle pairs, to describe the magnitude of activation a muscle shares with another. Muscle pairs (Table 5) were matched based on their line of action; some being synergists while others being antagonists. CCI calculations were performed for both experimental EMG activations and mean predicted muscle activations.

Table 5: Muscle pairs used for calculation of the co-contraction index.

Muscle 1	Muscle 2	Muscle Pair Abbreviation
Pectoralis Major	Infraspinatus	PEC-INFRA
	Latissimus Dorsi	PEC-LD
	Posterior Deltoid	PEC-PD
	Anterior Deltoid	PEC-AD
	Middle Deltoid	PEC-MD
Anterior Deltoid	Infraspinatus	AD-INFRA
	Latissimus Dorsi	AD-LD
	Posterior Deltoid	AD-PD
	Middle Deltoid	AD-MD
Middle Deltoid	Infraspinatus	MD-INFRA
	Latissimus Dorsi	MD-LD
	Posterior Deltoid	MD-PD

3.3. Statistics

To test the hypotheses, the predicted individual muscle activations from all 4 optimization functions (models) were cross correlated with experimental normalized EMG. The root mean squared difference (RMSD) between the magnitudes of the normalized predicted and experimental activities were also calculated. The average percent RMSD and explained variance (r^2) of each trial were compared for each model between different conditions using repeated measure (RM) ANOVAs.

The normalized EMG for the static trials was analyzed using a two-way repeated measures (RM) ANOVA. The independent variables where muscle (8) and duration of trial (25, 50, 75, and 100%) in order to observe if there were significant changes in muscle activity over the duration of the trials. Similarly an 8 × 3 × 4 RM ANOVA was used to compare the dynamic trials over the range of motion. The dependent variable was normalized EMG and the independent variables were muscle (8), plane (3), and angle (4).

A one-way RM ANOVA was used to compare the number of failed frames between models. Two 4 × 4 × 2 × 2 × 8 RM ANOVAs were used to compare the dependent variables RMSD and explained variance between multiple variables. The independent variables were model (squared, cubed, quartic, entropy), condition (fast, slow, static at 60°, static at 120°), force level (high, low), point of force application (upper arm, lower arm), and muscle (8 muscles). Since the stress test was performed at only one level of force and one point of force application it does not fit in the ANOVA. Two separate 4 × 5 RM ANOVAs were used to assess the RMSD and explained variance for the independent variables model (4) and condition (including the stress test).

To assess the models' abilities to predict co-contraction, a 5 × 12 RM ANOVA was used. The dependent variable was the CCI and independent variables were model (squared, cubed, quartic, entropy, and experimental EMG), and muscle pair (Table 5). A second 5 ×12 RM ANOVA assessed the differences in CCI between condition (5) and muscle pair (12).

The resultant JRF was divided into a resultant shear component (z and y) and compression component (x) for analysis. The magnitude of the shear/compression ratio (stability ratio) was calculated for each frame of each trial by dividing the shear component by the compression component of the JRF. The joint was considered stable or unstable based on the direction of the resultant shear force vector and the magnitude of the stability ratio compared to the dislocation force thresholds described by Lippitt and Matsen (1993). The thresholds are the amount of force required to translate the humeral head out of the glenoid fossa (shear) divided by the 100 N force (compression) applied to the head of the humerus during the translations.

The magnitude of the resultant JRF, shear force, and stability ratio was compared by using three 4 × 2 × 2 × 4 RM ANOVAs. The ANOVAs used the independent variables condition (4), force level (2), point of force application (2), and model (4). Another three 4 × 5 RM ANOVAs assessed the same dependent variables for the independent variables of model (4) and condition (5) to include the stress test in the analysis.

Mauchly's test for sphericity was performed for each RM ANOVA to test the null hypothesis that the variance of the differences is equal. A significant Mauchly's test indicated that sphericity was violated. When sphericity was violated, the Greenhouse-Geisser estimate was used to correct the degrees of freedom for the ANOVA to reduce the chance of type 1 error; if sphericity was maintained, the normal degrees of freedom were used. All significant main effects were followed up by Bonferroni corrected post hoc tests. All statistics were performed using SPSS software (IBM corp, Armonk, NY).

3.4. On Creating a Novel Shear Force Optimization Criterion

Significant time and effort were put towards adapting the existing model framework in OpenSIM to solve the muscle redundancy problem, by minimizing the shear forces instead of minimizing the sum of activations as seen in most models. By minimizing the shear forces, it was theorized that the predicted muscle activations would be closer to the experimental EMG, since stability plays a major role in shoulder muscle activations (Yanagawa et al, 2008; Ackland & Pandy, 2009). Attempts were made to adapt the properties of OpenSIM, SIMM, and the original version of the DSEM to accommodate such a function.

The first model adapted was the DSEM model implemented in the OpenSIM platform. This modeling platform uses a default optimization function that allows the user to change the power to which the sum of muscle forces is raised, and allows for the creation of optimization plugins, which modify the muscle activations (Macintosh, 2014). Attempts were made to adapt the code by changing the static optimization tool in OpenSim to minimize the sum of the shear joint reaction forces. The OpenSim interface was incapable of using an optimization function that minimizes any property other than muscle activation without a massive restructuring of the optimization tool, which was above and beyond the scope and level of this thesis.

The second model adapted was the original DSEM model. Changes were made to the optimization function file (objffsqp.f). The model would run when the power of the sum of muscle forces minimized and the coefficients of the metabolic cost function were changed but the model would not run when a novel optimization criterion was implemented. Lastly, an attempt was made to change the code using the dynamic module and SDFAST in the SIMM model of the DSEM, but with no success.

Based on the assortment of technical issues associated with implementing a novel optimization function to minimize shear forces, it was only feasible to investigate the optimization criterion which minimized muscle activation. Therefore, this thesis investigated four optimization models, the first three utilized the default static optimization function in OpenSIM to vary the power of the sum of muscle activations, and the fourth model used a recently created OpenSIM plugin (Macintosh, 2014) which minimized muscle activity based on an entropy-assisted optimization shown to invoke more co-contraction between muscles (Jiang & Mirka, 2007).

4. RESULTS

4.1 Modeling Summary

All trials collected (Table 1) were processed using the DSEM model in the OpenSIM modeling platform. Only the trials performed in the sagittal plane were successfully processed due to a limitation of the DSEM model that prevented analysis of abduction and scapular plane motions (further discussed in the limitations section). Thus, all of the results presented apply to the shoulder flexion trials collected in the sagittal plane. Each trial was processed using four different optimization criteria, these criteria will further be referred to as the Σa^2 model (sum of squared activations), Σa^3 model (sum of cubed activations), Σa^4 model (sum of quartic activations), and the entropy model (entropy-assisted model). Participant anthropometry (Table 6), as well as marker data, were used to linearly scale the DSEM model for each of the participants before performing inverse kinematics, inverse dynamics, and static optimization.

Table 6: Participant anthropometrics, n=10 (mean with standard deviation).

Age (yr)	Weight (Kg)	Height (m)	Total Arm Length (m)	Upper Arm Length (m)	Lower Arm Length (m)
22.7 ±2.1	74.7 ±8.8	1.74 ±0.05	0.56 ±0.052	0.30 ±0.03	0.25±0.02

The inverse kinematics tool (OpenSIM) reached a solution for all trials based on the recorded marker positions and calculated joint angles. However, the static optimization tool did not. The static optimization tool was first used without aid of residual actuators and failed to reach a solution for all trials due to the inherent maximum muscle forces of the muscles in the OpenSIM model being too “weak” and unable to generate moments to drive the action. This occurs mainly when angular accelerations are high requiring short bursts of muscle activity. To add "strength" to the model consistently, reserve torque actuators were set at each degree of freedom in the model to generate torque when the muscles alone cannot produce enough force to generate the moments. The maximum allowable contribution of reserve torque actuators (at each joint in the model) was set to 30 Nm (van der Krogt et al, 2012; Steele et al, 2012). After the reserve actuator file was appended, only 3 out of 170 trials (total for all participants) failed to converge a solution. It was possible for trials to not fail completely but have failed frames. A failed frame occurred when a solution was unable to be found, or a solution was found but constraints were broken to achieve it. A one-way RM ANOVA demonstrated a significant difference in failed frames between models ($F_{1.616, 14.543}$ = 3351.347, $p<0.001$). Bonferroni corrected post hoc tests indicated that the entropy model had a significantly higher percent of failed frames (99.5 ± 0.6%) than all three sum of activations models ($p<0.001$), and the sum of squared activations (1.8 ± 4.0%) had a significantly lower percent of failed frames than the sum of cubed activations (3.3 ± 4.1%) and sum of quartic activations (5.5 ± 5.2%) ($p<0.05$). This suggests the more an optimization promotes muscle load sharing the more inclined it is to have failed frames because co-activation of muscles increases the force needed from muscles to produce the same net moment at a joint. Typically when a frame failed, there would be a zero or "NaN" value for the muscles, or if a group of frames failed the muscle activations would turn on and off sharply between consecutive frames jumping from maximum activation to zero activation. The entropy model had approximately 99% of frames fail for most trials but OpenSIM would output muscle activations not typical of a failed frame. The frames would have values for every muscle and would not sharply jump from maximum to zero muscle activation between consecutive frames. After visual observation the activations of the frames had a similar pattern to frames that did not fail, therefore the data were included in the statistical analyses.

Each scaled model was computed using 4 different optimization criterions, as described in the Methods. The RMSD and explained variance (r^2), between the normalized predicted activation and normalized experimental EMG, were calculated for each muscle to assess the differences in magnitude and shape for each model. Overall, the sum of activation models explained significantly more variance, and had significantly lower RMSD between experimental and predicted activities, compared to the entropy model ($p<0.01$). More specifically the sum of cubed and sum of quartic models explained the most variance in EMG ($p<0.01$) (Table 7).

Table 7: Mean RMSD and mean, maximum, and minimum explained variance for each model presented with standard deviation. (*significantly larger, p<0.01, **significantly larger, p<0.01)

	Σa^2 Model	**Σa^3 Model**	**Σa^4 Model**	**Entropy Model**
RMSD (%)	17.85 ±13.77	17.27 ±12.73	17.26 ±12.30	22.01 ±9.66*
Explained. Variance (r^2)	0.37 ±0.26	0.38 ±0.25**	0.38 ±0.25**	0.14 ±0.14
Max Explained Var. (r^2)	0.98	0.98	0.98	0.88
Min Explained Var. (r^2)	0.0025	0.0025	0.0025	0.0081

4.2. EMG & Model Evaluation

The models were compared to the experimentally recorded EMG from several muscles for all conditions. The mean recorded EMG activation for each muscle during each condition (Figure 16) in all three planes is reported in Appendix A. The recorded EMG stayed fairly constant over the 3 sec portion of the static trials used for model comparison. The EMG showed no significant interaction or significant differences over the duration of the static trials for any muscles. The dynamic trials were also compared over the duration of the trial (0-120° range of motion). There was a significant muscle by plane interaction ($F_{3.418,30.76.} = 4.941$, $p<0.01$) as well as a muscle by angle interaction ($F_{3.875,34.847.} = 12.779$, $p<0.01$). After post hoc testing it was seen that the middle deltoid demonstrated significantly more activation during abduction than any other plane ($p<0.01$). It was also seen that pectoralis major demonstrated significantly more activation during flexion in the sagittal plane than any other planes ($p<0.05$). When observing the EMG over the range of motion it was also found that the EMG collected at 90° and 120° was significantly greater than EMG at 30° and 60° for all muscles other than pectoralis major. The pectoralis major showed a general trend to decrease its activity above 90°. This suggests there is an increased need for muscle activity when the arm is elevated above 90°.

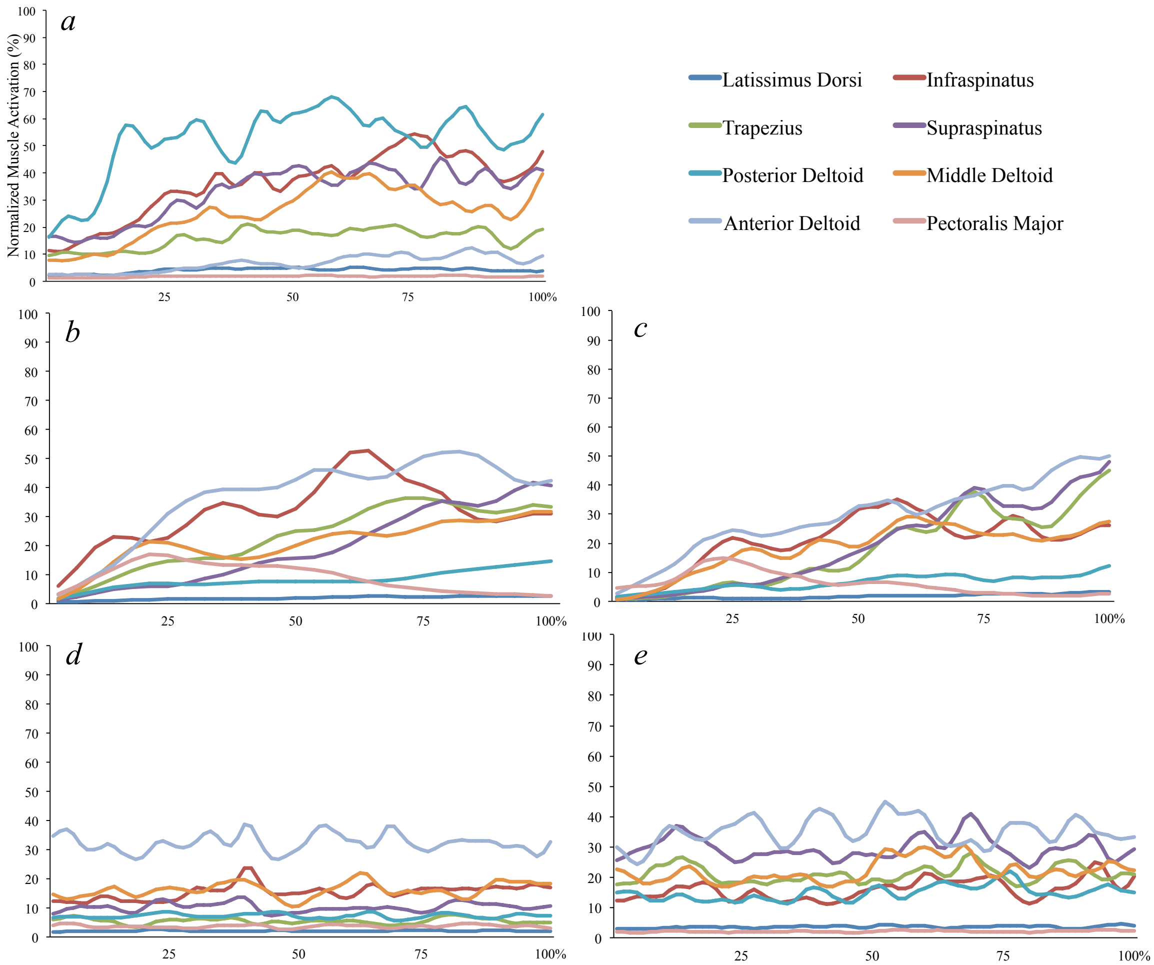

Figure 16. Subject 5 normalized EMG recordings in the sagittal plane for the conditions; *a*) stress test, *b*) dynamic 120°/s, *c*) dynamic 60°/s, *d*) static 60°, *e*) static 120°. Each chart illustrates the recorded muscle activations over the duration of the trial.

The explained variance (r^2) from a cross correlation between predicted and experimental activations was compared between models (4), conditions (4), forces (2), points of force application (2), and muscles (8). Mauchly's test indicated the assumption of sphericity was violated for the main effects of model, force, and point of force application. A significant interaction was seen between models and muscles ($F_{5.152, 46.369} = 5.526$, $p<0.01$). After Bonferroni corrected post hoc tests models Σa^2, Σa^3, and Σa^4 were seen to predict significantly more variance for all muscles when compared to the entropy model ($\Delta r^2 = 0.22 \pm 0.03$, $p<0.01$). Model Σa^3 explained more variance than model Σa^4 for trapezius upper fibres ($\Delta r^2 = 0.02$, $p<0.05$), and model Σa^4 explained more variance than model Σa^2 for supraspinatus ($\Delta r^2 = 0.03$, $p<0.05$) (Figure 17).

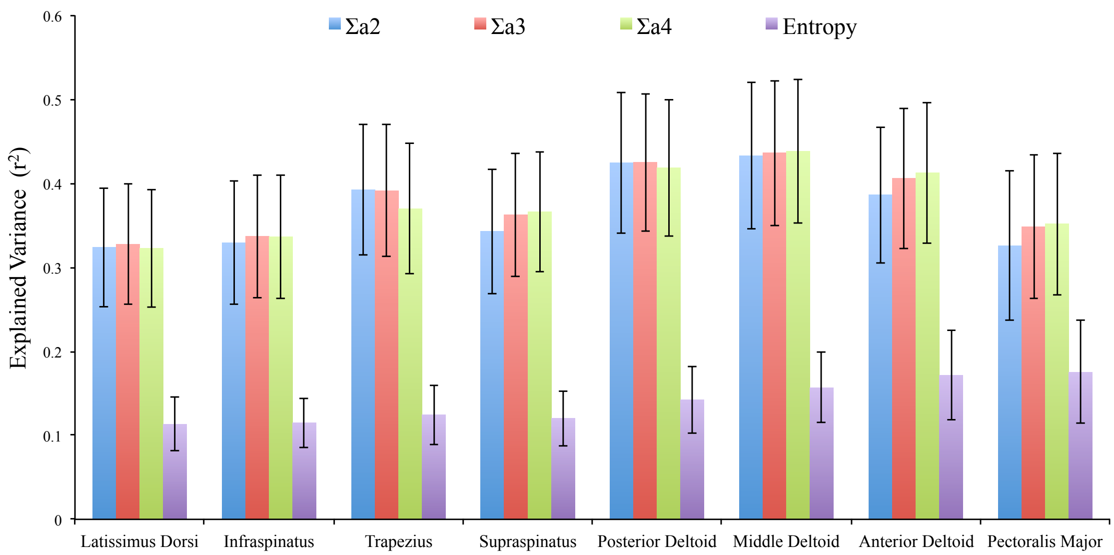

Figure 17. Mean explained variance across all tasks, between experimental and predicted muscle activations, for each muscle within each model (error bars represent standard error).

The RMSD between normalized experimental EMG and predicted muscle activities was compared using a five-way ANOVA between models (4), conditions (4), forces (2), points of force application (2), and muscles (8). Mauchly's test indicated the assumption of sphericity was violated for the main effects of several independent variables therefore degrees of freedom were corrected using Greenhouse-Geisser estimates for these variables. Significant three-way interactions were seen between model, condition, and muscle ($F_{6.029, 54.263} = 5.673$, $p<0.001$), as well as model, force, and muscle ($F_{3.422, 30.802} = 16.149$, $p<0.001$). After Bonferroni corrected post hoc testing, it was found for models Σa^2, Σa^3, and Σa^4 regardless of condition the supraspinatus and pectoralis major muscles had an average of 17.31 ±5.2 greater RMSD between experimental and predicted activity than latissimus dorsi and posterior deltoid ($p<0.01$). During static 120° trials, supraspinatus was predicted to have significantly higher RMSD than latissimus dorsi, infraspinatus, trapezius upper fibres, posterior deltoid and middle deltoid for the same three models ($p<0.01$). The entropy model showed pectoralis major to have significantly higher RMSD than latissimus dorsi and posterior deltoid across all conditions, which was similar to the three sum of activation models ($p<0.01$). Thus, the model activity predictions seem to have a higher percent error compared to EMG when the muscle in question was an agonist, and less error when the muscle was an antagonist during shoulder flexion. (Figure 18).

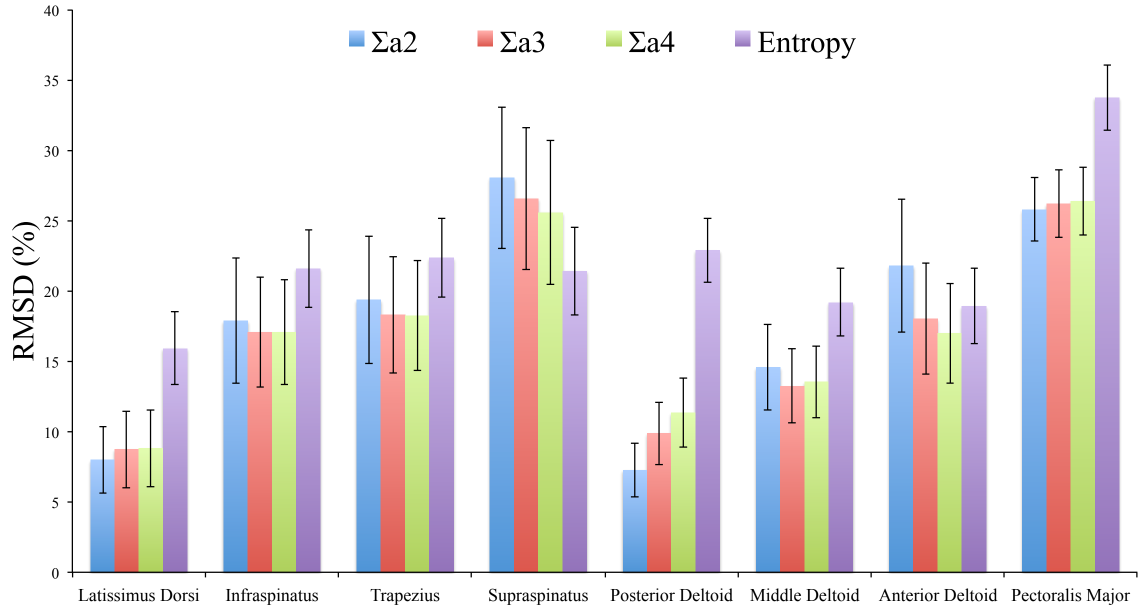

Figure 18. Overall Mean RMSD between experimental and predicted muscle activations for each muscle within each model during shoulder flexion (errors bars represent standard error). Major agonists include the anterior deltoid, and pectoralis major. Minor agonists include middle deltoid, trapezius, and supraspinatus.

For models Σa^2, Σa^3, and Σa^4, during high force trials, supraspinatus showed a higher RMSD (19.8 ±6.7%) between experimental and predicted activities than most of the muscles (latissimus dorsi, infraspinatus, posterior deltoids and middle deltoids) ($p<0.01$). When the same models were used to predict low force conditions, pectoralis major showed higher RMSD (16.2 ±4.3%) than latissimus dorsi, infraspinatus, posterior deltoids, and middle deltoids ($p<0.01$) for models Σa^2, Σa^3, and Σa^4.

Two RM ANOVAs were used to investigate the model predictions during the different conditions. The first compared the explained variance between predicted and experimental muscle activities and the second compared percent RMSD. Mauchly's test indicated a violation in sphericity for the main effect of models but sphericity was not violated for the main effect of conditions. After a Greenhouse-Geisser correction, a significant interaction was seen between models and conditions ($F_{2.405, 21.649} = 7.036$, $p<0.01$). The sum of activation models explained significantly more variance than the entropy model for each condition ($\Delta r^2 = 0.22 \pm 0.04$, $p<0.01$), and model Σa^3 explained significantly more variance than model Σa^2 during the static 120° condition ($\Delta r^2 = 0.02$, $p<0.01$). The entropy model explained significantly more variance for the fast trials compared to both of the static conditions as well as the stress test (apprehension position) ($\Delta r^2 = 0.12 \pm 0.01$, $p<0.01$), and slow trials predicted significantly more variance than the static conditions ($\Delta r^2 = 0.08$, $p<0.05$). This suggests that the amount of explained variance in EMG based on the entropy model predictions is increased when the model is used to predict dynamic movement but no such differences were found between the sum of activation models (Figure 19).

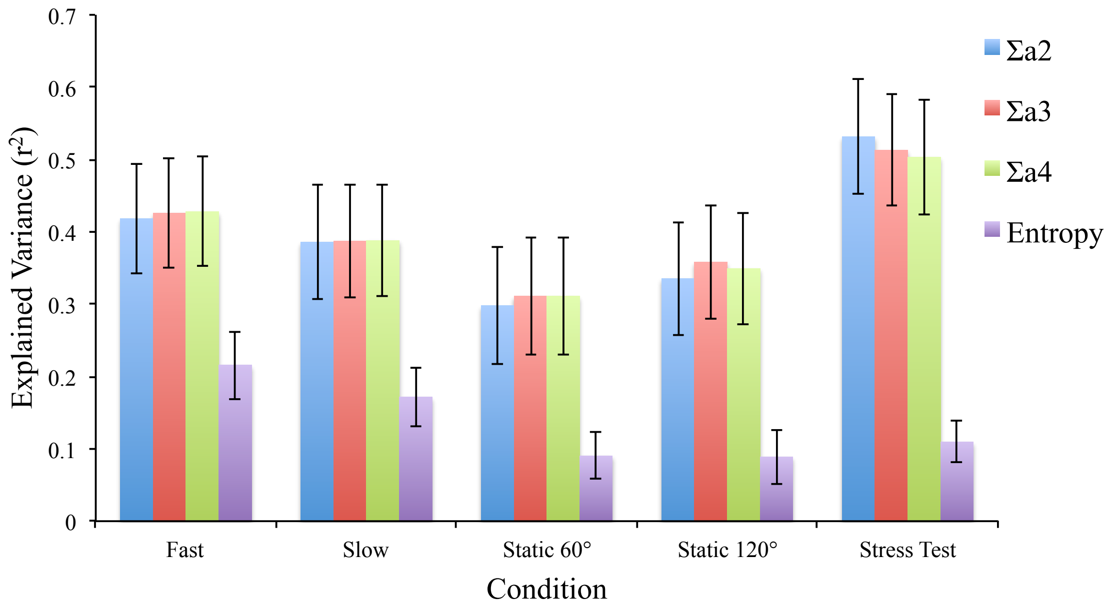

Figure 19. Mean of all muscles explained variance for each model during each condition. (error bars represent standard error).

A significant model by condition interaction was seen ($F_{2.235, 20.116} = 7.953$, $p<0.01$) for percent RMSD between normalized experimental and predicted activity. Bonferroni corrected post hoc testing of the interaction indicated significantly higher RMSD for the entropy model compared to the three sum of activation models for the slow and static 60° conditions (Δ7.9 ±3.6%, $p<0.05$). Model Σa^2 was seen to have significantly higher RMSD when compared to model Σa^3 and model Σa^4 for the static 120° condition (1.4 ±3.6%, $p<0.01$). Model Σa^4 was seen to have significantly higher RMSD than model Σa^2 for the static 60° condition (Δ1.3%, $p<0.01$) (Figure 20).

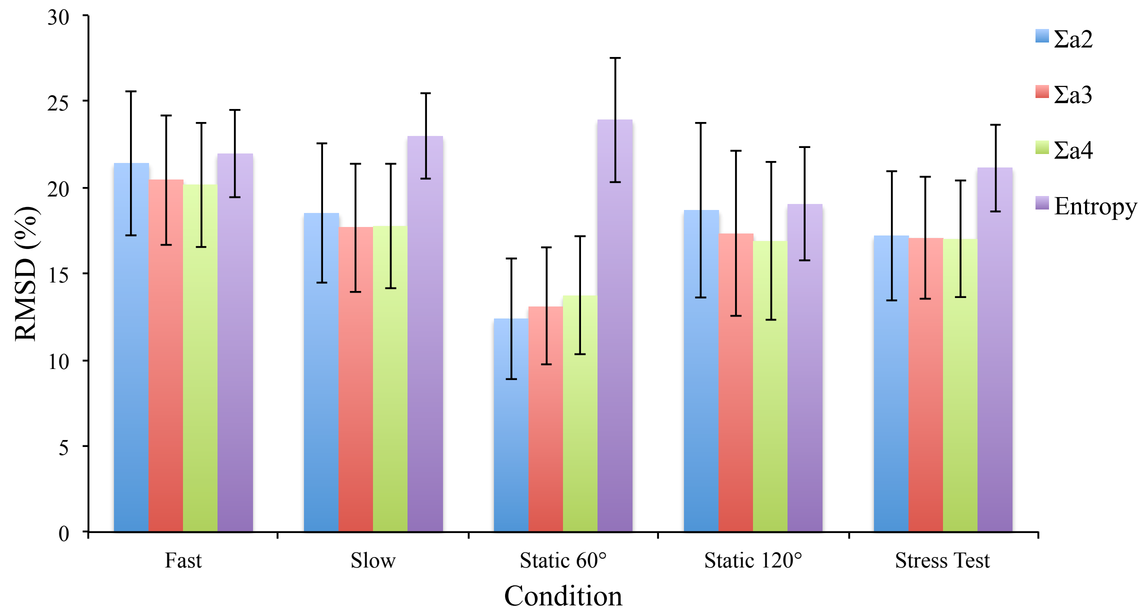

Figure 20. Mean of all muscles RMSD between experimental and predicted muscle activity in each condition for each model (error bars represent standard error).

4.3. Co-Contraction Index

A co-contraction index was used to quantify the similarity in activity between specific muscle pairs (Table 5) for both the experimental and predicted muscle activities. Mauchly's test revealed a violation in the assumption of sphericity for all main effects. A significant interaction was seen between CCI source and muscle pair ($F_{4.986,\, 44.878}$ = 15.692, p<0.001). As expected the entropy model had a significantly higher CCI than models Σa^2, Σa^3, and Σa^4 for every muscle pair (Δ0.412 ± 0.14, p<0.01). The CCI of the experimental EMG was significantly higher than models Σa^2, Σa^3 , and Σa^4 for the muscle pairs involving latissimus dorsi (Δ0.091 ± 0.02, p<0.05), and significantly higher than models Σa^2 and Σa^3 for the muscle pairs involving infraspinatus and the anterior and middle deltoid muscles ($\Delta 0.22 \pm 0.04$, $p<0.05$). Although models Σa^2, Σa^3, and Σa^4 predicted significantly lower CCI between some antagonistic muscle pairs, the models predicted significantly higher CCI for the anterior and posterior deltoid muscle pair. This suggests that models Σa^2, Σa^3, and Σa^3 predict co-activation poorly for some antagonistic muscle pairs but better for others (Figure 21).

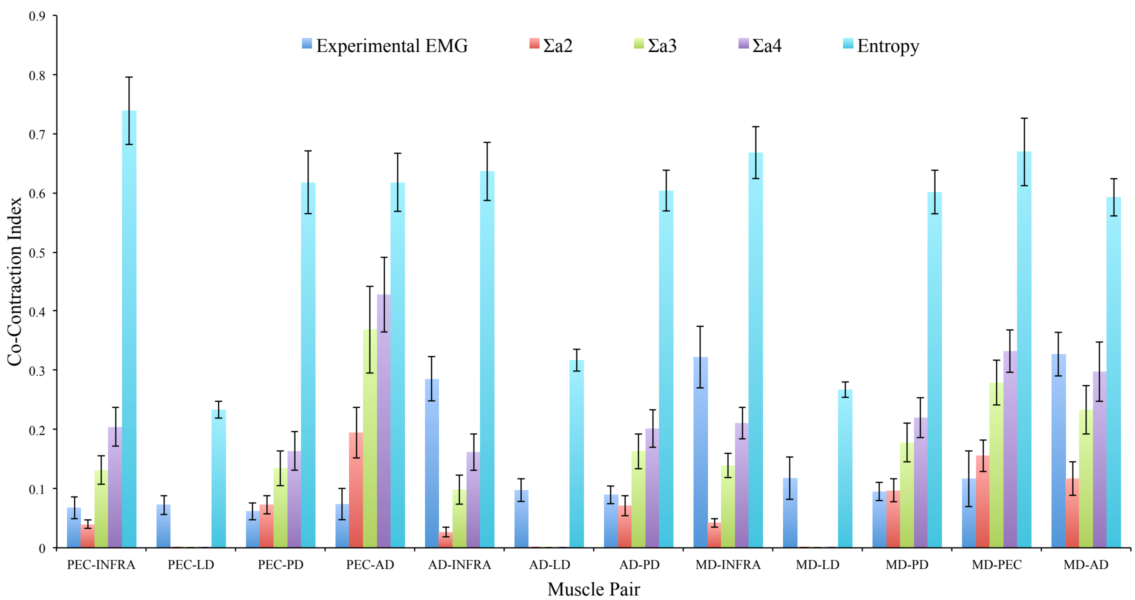

Figure 21. Predicted and experimental CCI with standard error for all 12 muscle pairs; PEC= pectoralis major, INFRA= infraspinatus, LD= latissimus dorsi, PD= posterior deltoid, AD= anterior deltoid, MD= middle deltoid (error bars represent standard error).

A significant interaction between conditions and muscle pairs was observed when assessing differences in CCI ($F_{44, 396} = 1.638$, $p<0.01$). Divergent from the hypothesis, the fast condition was seen to have significantly higher CCI than both static trials and the stress test for the muscle pairs; PEC-AD, AD-INFRA, MD-INFRA, and MD-AD (Δ0.15 ± 0.03, $p<0.05$). The fast condition was also seen to have significantly higher CCI than the stress test for the muscle pairs; AD-PD, and MD-PEC (Δ0.067 ± 0.004, $p<0.05$). The slow condition showed a significantly higher CCI than both the static conditions and the stress test for multiple muscle pairs (PEC-AD, AD-INFRA, MD-INFRA, MD-PEC) (Δ0.091 ± 0.02, $p<0.05$). This indicates there is more co-activation in dynamic tasks when compared to static tasks for most muscle pairs (Figure 22).

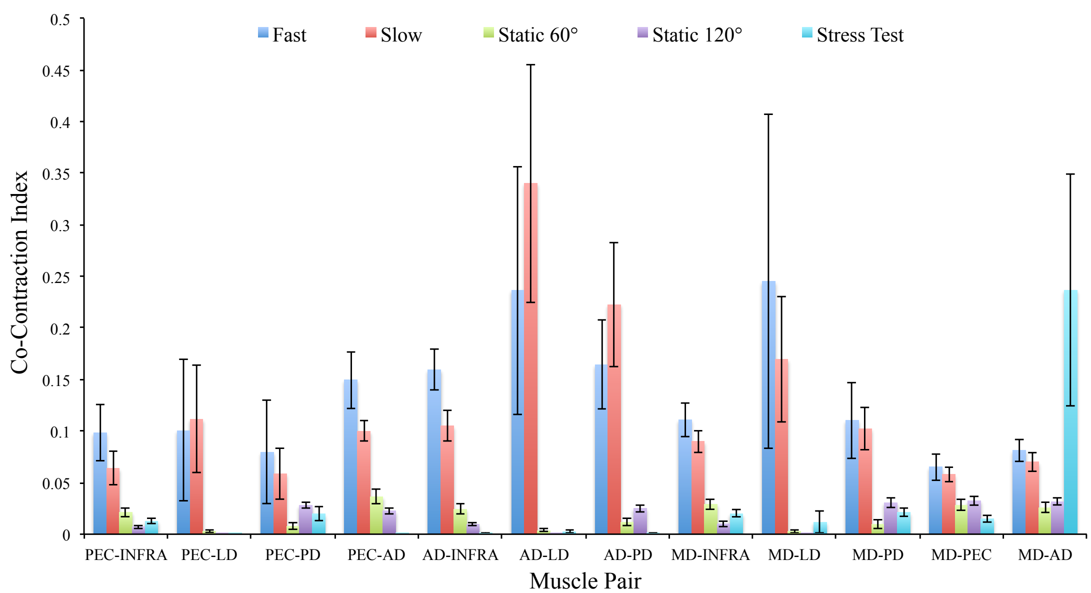

Figure 22. Average CCI and standard error of muscle pairs for each condition; PEC= pectoralis major, INFRA= infraspinatus, LD= latissimus dorsi, PD= posterior deltoid, AD= anterior deltoid, MD= middle deltoid (error bars represent standard error).

4.4. Joint Reaction Force

The predicted magnitude of shear forces, resultant JRFs, and the stability ratio (shear/compression) were investigated for the different conditions. After correction for sphericity, the only significant main effect for the shear forces and resultant JRFs was between models ($F_{1.002, 9.017} = 19.361$, $p<0.01$; $F_{1.004, 9.034} = 23.558$, $p<0.01$). Post hoc testing for both RM ANOVAs indicated that the shear forces and JRFs increased significantly with the power of the sum of activation model used ($p<0.01$), and the entropy model predicted significantly more force than all three sum of activation models ($p<0.01$) (Figure 23). No significant main effects were found for the stability ratio (SR).

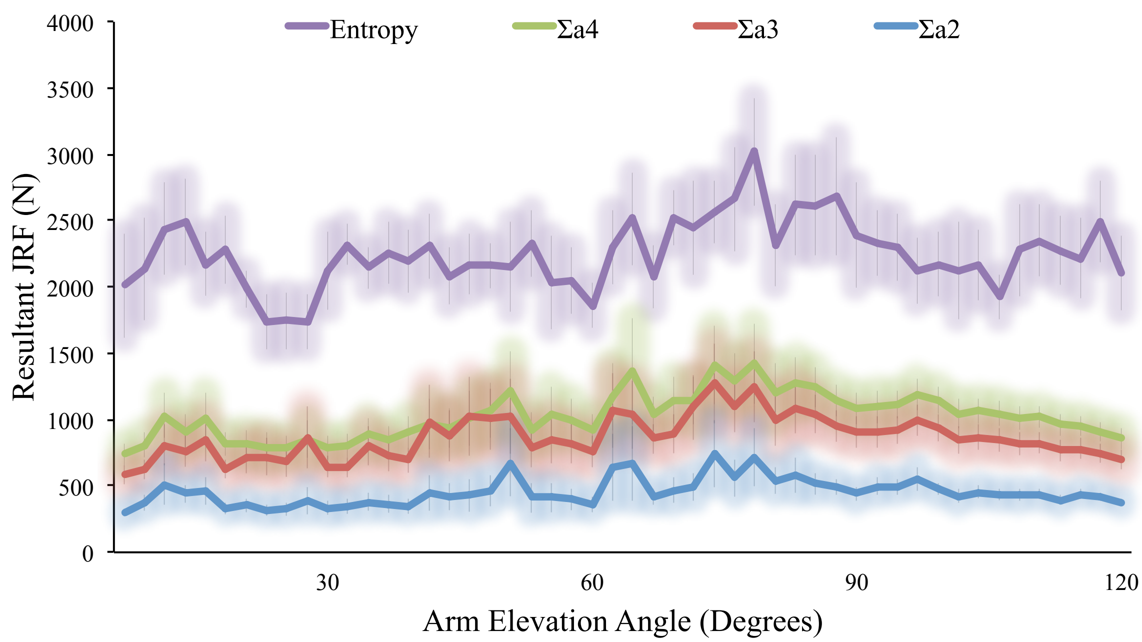

Figure 23. Mean resultant JRFs for sum of activation models and entropy-assisted model over duration of slow flexion trial (shadow represents standard error).

Two RM ANOVAs were used to investigate shear force, resultant JRF and the stability ratio for the independent variables model (4) and condition (5). Significant differences in shear force were found between conditions ($F_{1.480,\ 13.321} = 6.544$, $p<0.05$). Post hoc testing indicated the stress test had significantly lower shear force than the fast, slow, and static conditions ($p<0.01$). No significant main effects were found for the stability ratio and no significant differences in resultant JRF magnitude were seen between conditions. On average, the glenohumeral joint was unstable (SR > dislocation threshold) but the joint was seen to be the most unstable when the arm was above 90° of shoulder flexion (Figure 24).

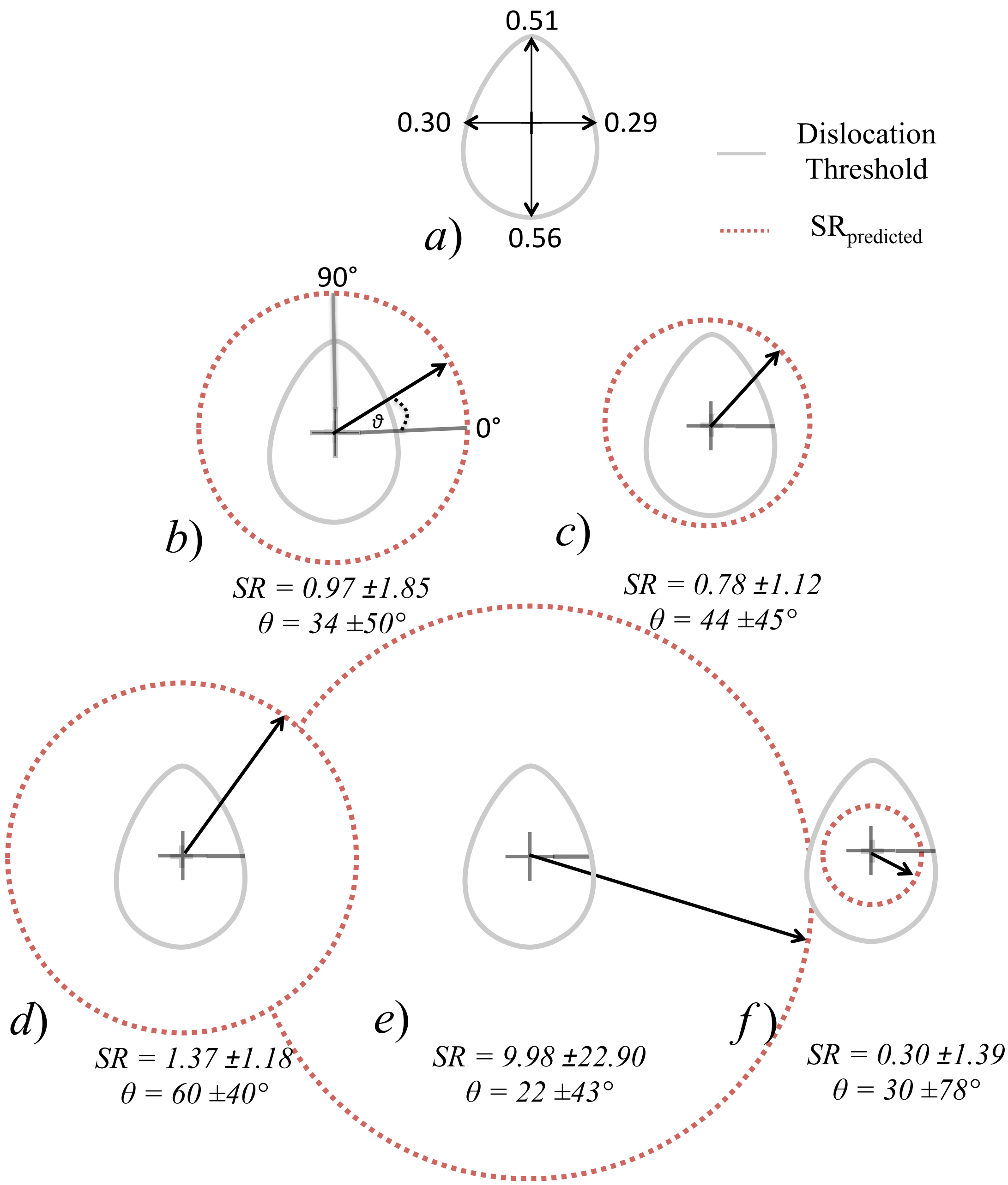

Figure 24. The average stability ratio (SR) and standard deviation of each condition as well as direction of shear force (*θ)* and standard deviation; *b*) Fast, *c*) Slow, *d*) Static 60°, *e*) Static 120°, *f*) Stress Test. The grey oval represents the dislocation threshold (threshold levels described in *a*)., the red ring represents the conditions average SR, and the arrow represents the direction of the shear force. Note, the static 120° SR is not seen to scale as it is much larger than the other ratios.

5. DISCUSSION

This thesis provides insight into the performance of four available optimization functions for prediction of muscle activity over a variety of shoulder movements and positions. Using an open source musculoskeletal model it was found that as the power of the sum of activation models was increased the model predicted more co-activation of muscles and the sum of cubed and quartic activation models explained more variance than the sum of squared model in the collected EMG. The EMG demonstrated higher muscle activity is needed when the arm is raised above 90°. The models also predicted the GH joint to be less stable at higher arm elevations. Combining the EMG and stability results demonstrates more co-activation is needed from muscles surrounding the GH joint for stabilization when the arm is above 90° of elevation.

5.1. Model Summary

The first purpose of this thesis was to compare the performance of the different optimization criteria (models) available in OpenSIM for the DSEM model. Overall, the models did not predict muscle activation as well as expected for the entire sample population. The models predicted some trials very well resulting in explained variance of 98% but the models also predicted very poorly for other trials with explained variances of less than 1%. The sum of activation models did not differ significantly from each other in their predictions of muscle activation magnitude, but, as expected, the cubic and quartic functions performed better at predicting muscle activation shape most likely due to the equations predicting more muscle co-activation.

The entropy model predicted higher activity than any of the sum of activation models and over predicted when compared with experimental EMG data, but this model also resulted in the highest number of failed frames. After rerunning the entropy model for a sample of trials from different participants with the reserve actuators set to 1000 Nm instead of 30 Nm, the percent of failed frames decreased significantly to less than 50% for each trial. This suggests the model was too "weak" to run the entropy-assisted static optimization function. This is most likely due to the nature of the optimization function, in that the added entropy term helped predict more co-activation than the other models. This in turn resulted in higher muscle activity for all muscles surrounding the joint, since more force is needed to create the same moment when antagonistic muscles are active. In most cases the model predicted much higher activity than seen experimentally, but after testing a sample of trials with a decreased weight factor W in the entropy term, the degree of co-contraction was lessened resulting in lower predicted activations.

The sum of muscle activity equations tended to predict higher activity when a higher power was used (Figure 25). This could be related to the amount of muscle load sharing or co-activation occurring at the GH joint. As the power of the optimization function increases the load sharing increases, since the higher power puts less emphasis on the size of the muscles moment arm when choosing muscles to converge on a solution (Dul et al, 1984). When the power of the equation is increased the contribution of each muscle is limited therefore activating more muscles to produce the same moment. As more muscles are recruited some antagonists are also activated. When more antagonists are actively opposing a motion, the agonists must increase their activation to produce a given net moment. Therefore increased co-activation of muscles leads to higher predicted activity.

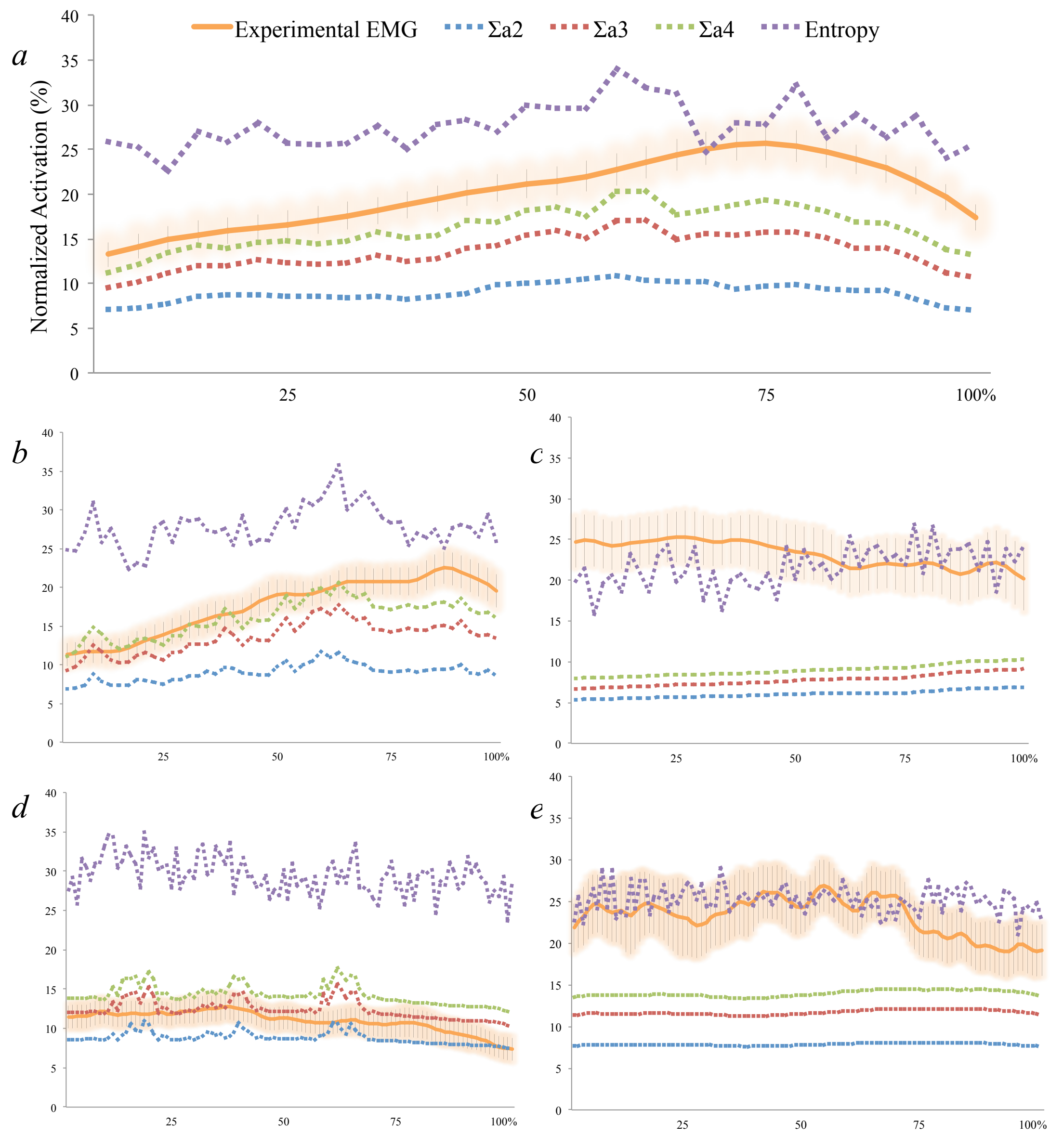

Figure 25. Normalized experimental activations (all muscles averaged) and predicted muscle activations for each model and each trial condition (*a,b,c,d,e*) averaged across all participants. The experimental activation traces are shadowed with the standard error. (*a*) the average activation of all fast trials over the duration of the recorded movement (0%=0°, 100%= 135°). (*b*) the average activations of all slow trials, (*c*) the average activations of stress test, (*d*) average activations of static 60° trials, and (*e*) average activations of static 120°.

Overall, there were a few differences seen across the conditions. The fast trials had significantly greater RMSD than the static trials, suggesting the accuracy of the model may decline with increasing speed. The sum of activation models did not perform significantly different for the stress test (apprehension position) compared to any of the other conditions, and there were no significant effects based on the location of force application.

Some muscles magnitude of activity was better predicted than others. Supraspinatus, pectoralis major, and anterior deltoids had significantly higher RMSDs than latissimus dorsi and posterior deltoid for all conditions and all sum of activation models. The entropy model showed similar results, pectoralis major had a significantly higher RMSD than latissimus dorsi and posterior deltoid across all conditions. This indicates that there was more error in predicting agonists than antagonist muscles, but the errors may be larger in agonists given that they had higher activity than antagonistic muscles. Having higher absolute activity makes them susceptible to greater error when compared to muscles with an activation of zero or close to zero.

The mean correlations between predicted and experimental EMG for each muscle were slightly higher than those seen in a previous study involving the DSEM model implemented in OpenSIM (Blana et al, 2008), but slightly lower than those from a study using the original DSEM model not implemented in OpenSIM (Nikooyan et al, 2011) (Table 8). Blana et al (2008) observed a wide variety of movements including abduction/adduction in the frontal, scapular, and sagittal planes, horizontal flexion/extension, internal and external rotation, elbow flexion/extension, forearm pronation/supination and some activities of daily living. Nikooyan et al (2011) observed slow flexion motions in the sagittal plane similar to those completed in this thesis, but they were only completed for one patient with shoulder hemi-arthroplasty.

Table 8: Average correlation coefficients for all trials compared to literature.

	Correlation Coefficient (R)
Model Σa^2	0.57 ±0.22
Model Σa^3	0.58 ±0.22
Model Σa^4	0.57 ±0.22
Entropy Model	0.34 ±0.16
Blana et al (2008)	0.46
Nikooyan et al (2011)	0.71

5.2. Co-Activation

It has been demonstrated that the surrounding musculature at the shoulder actively work to increase the stability of the glenohumeral joint (Itoi et al, 1996, Lippitt & Matsen, 1993; Culham & Peat, 1993; Kronberg et al, 1990). To balance the shear forces occurring at the glenohumeral joint, co-contraction of muscles is required. Co-contraction is usually described as the simultaneous activation of an agonist and antagonist muscle (Nikooyan et al 2012; Gribble et al, 2003). Unlike a hinge joint, such as the elbow which is stabilized mainly through antagonistic activation, the shoulder is stabilized by antagonistic and synergistic activation of many surrounding muscles working in concert with each other. Thus, stabilization at the shoulder occurs through co-activation of muscles, including antagonistic and synergistic muscle activity. The sum of activation models predicted similar levels of synergistic muscle co-activation but predicted significantly less antagonistic activation when compared to experimental EMG.

Muscle pairs (Table 5) were chosen based on their line of action and relative contribution to the torque production of the arm during shoulder flexion. The anterior deltoid and pectoralis major were seen as the major agonists and the latissimus dorsi and posterior deltoid were seen as the major antagonists during shoulder flexion (Wattanaprakornkul et al, 2011). Infraspinatus was a significant stabilizer and middle deltoid was seen as a minor agonist, therefore they were included in the muscle pairings as well. It should be noted that pectoralis major was considered an agonist from 0-90° and an antagonist above 90° for shoulder flexion, the EMG showed the activity of pectoralis major to increase until just before 90° and then decline in activity after 90°. The co-contraction index was compared between models in order to investigate the second purpose of this thesis. The co-contraction index is not a new equation, but it has yet to be seen used for muscles of the shoulder complex. Experimental EMG for muscle pairs involving latissimus dorsi had significantly higher CCIs than all sum of activation models. In addition, models Σa^2 and Σa^3 under predicted co-activation between infraspinatus and the anterior/middle deltoids. This indicates the sum of activation models predict antagonistic co-activation poorly. Conversely the models show higher co-activation than experimental EMG when comparing pectoralis major and posterior deltoid, as well as anterior deltoid and posterior deltoid suggesting the models predict some antagonistic co-activation (Figure 21). Supporting Dul et al (1984), there was significantly more co-activation predicted when the power of the sum of activation model was increased.

Contradictory to the second hypothesis, the stress test (apprehension position) showed significantly less co-activation (CCI) when compared to the dynamic trials. This might be attributed to the differences in which muscles were active during the flexion movement and the apprehension position as well as the nature of a dynamic movement compared to a static position (flexion performed as dynamic arm elevation and apprehension was static external rotation). The lower CCI could also be attributed to the increased capsuloligamentous support of the shoulder in the end range of motion (Lee et al, 2000; Kronberg et al, 1990). The fast and slow conditions also showed significantly higher CCIs than the static conditions for most muscle pairs indicating more co-activation is needed to stabilize a moving joint than one which is static, most likely due to the need for increased stability when there is a greater possibility for the humeral head to translate in the glenoid. The movements angular accelerations (especially at the beginning and end range of movements) could also cause increased co-activation of muscles.

5.3. Joint Reaction Force

Joint reaction forces were reported in three ways, (i) the magnitude of shear force, (ii) the magnitude of resultant JRF, and (iii) the stability ratio (shear/compression). To create two shear force conditions, two points of force application were used during data collection. One location was on the upper arm and the other was on the lower arm (Figure 9). Changing the length of the moment arm, but maintaining the torque produced by the arm, creates two levels of shear force seen at the joint (Aalbersberg et al, 2005). A significant difference in predicted shear force at the GH joint was not seen between the two loading positions as expected. This could be due to the moment at the shoulder not staying completely constant (even though the dynamometer was used in isotonic mode), but it is more likely because the entire arm is not a rigid body due to the elbow joint. The arm was fully extended for all conditions (except stress test) but the biarticular muscles of the shoulder and elbow flexors, such as the biceps brachii, may have been more active when the point of force application was distal to the elbow adding force and lessening the effect of the two shear conditions.

Lippitt & Matsen (1993), as well as Yanagawa et al (2008), have shown that the co-activation of surrounding musculature can act to lower the shear force at the glenohumeral joint. The stress test (apprehension position) had significantly lower shear force than the fast, slow, and static conditions, yet both dynamic conditions predicted significantly more co-activation than the stress test. This could be attributed to the differences in arm posture between the stress test and arm flexion, the stress test was performed as a static contraction with a combination of an external rotation and horizontal extension movement close to the shoulders end range of motion. This could also be attributed to the fact that the models predicted significantly less total activation for the stress test compared to all other conditions.

Since muscle activity surrounding the joint was seen to increase the JRF, less activity of the surrounding musculature in the apprehension position resulted in lower JRFs at the glenohumeral joint. The JRFs were lower since there was less force from the muscles pulling the head of the humerus into the glenoid. There was a significant difference found in shear force between models, as the power was increased in the sum of activation models, the amount of shear force also increased. Similarly, predicted co-activation increased with the power of the function. It is proposed that the models artificially predicted more shear force with increased co-activation based on the premise that increased co-activation would also increase the resultant JRF magnitude predicted by the model. To address this conflict, the average shear force was normalized to the resultant JRF. After normalizing, a general trend showed the shear force component decreased with respect to the total resultant JRF magnitude as more co-activation was predicted, coinciding with the literature (Lippitt & Matsen 1993; Yanagawa et al, 2008; Ackland & Pandy, 2009). By co-activating surrounding muscles the compression component of the JRF is increased and the muscle forces are more balanced around the joint similar to guide wires around a radio tower, this causes less shear force at the joint and increases stability.

The stress test had significantly lower shear force with no differences in resultant JRF between conditions. Based on these findings, we would expect the stability ratio for the stress test to be significantly less than the other conditions, indicating that it is more stable. The stress test was seen to generally have a lower stability ratio than other conditions but significance was not found. The stability ratio did not differ significantly between models, or between conditions. This may be due to the high variability in the stability ratios. The mean stability ratio was generally seen to be higher for the static 120° condition which implies there is less stability when the arm is above shoulder height.

Nikooyan et al. (2010) compared JRFs predicted and measured *in vivo* from instrumented endoprostheses in two osteoarthritic patients. The results of their *in vivo* force measurements, and muscle stresses squared predictions for a slow flexion movement were compared with the sum of activations squared predictions for the slow flexion movement performed in this thesis (Figure 26). The sum of squares model was compared, as it is analogous with the sum of muscle stresses squared model. Their study showed greater differences between the measured and predicted JRF when the shoulder was above 90°. The study found that, as the arm moved past 90° of flexion, the model would predict a decrease in JRF but the measured JRF from the prosthesis still increased (Figure 26). This decrease in predicted force was also reported during abduction (Poppen & Walker, 1978). Poppen & Walker (1978) attributed the decrease to the muscle moment arms. At 90°, the moment arms for the muscles in their model (three deltoids and supraspinatus) were at their maximum, therefore the moment arms and JRF subsequently decreased at angles greater than 90°. My study found the mean resultant JRF for the sum of squared activation model to slightly decrease after 90° of flexion similar to Nikooyan et al (2010), but the cubic and quartic functions as well as the entropy model generally stayed constant over the range of motion (Figure 26). This may again be attributed to the ability of the two models to predict more co-activation than the sum of squares model.

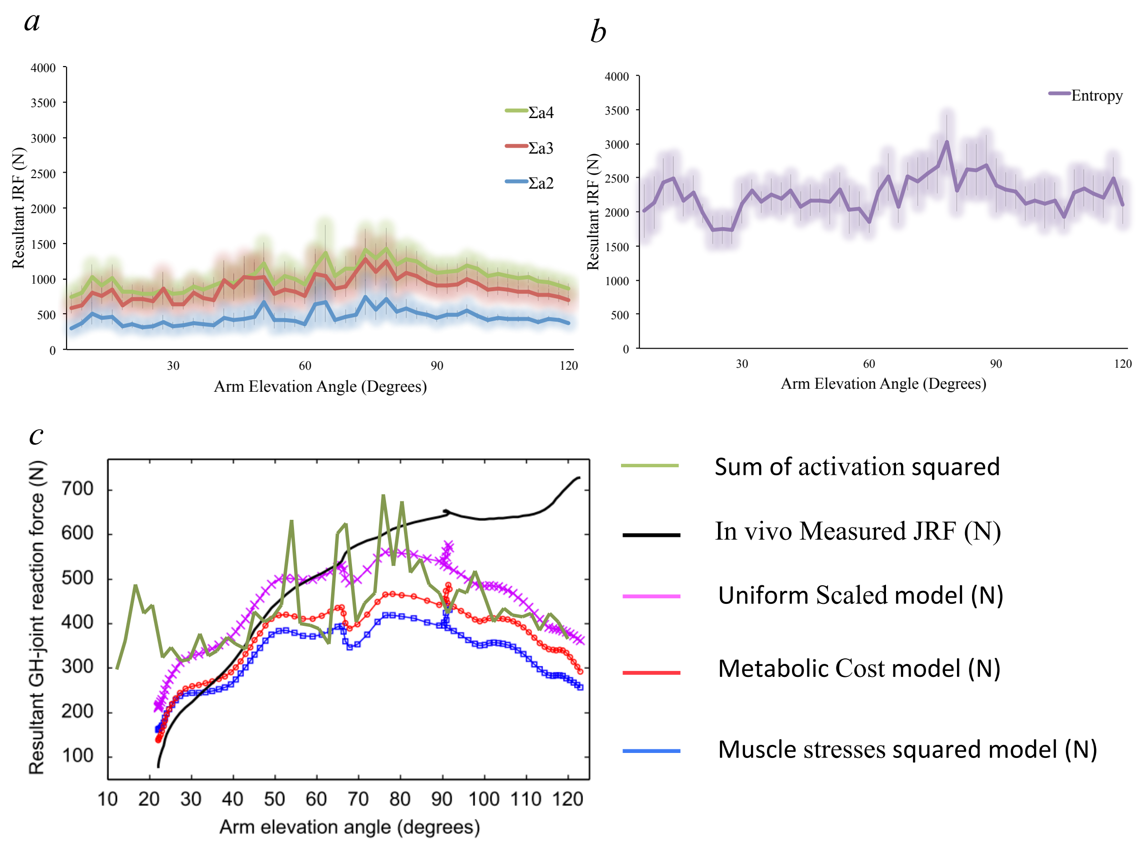

Figure 26. Resultant JRFs presented with standard error for the sum of activation models (*a*), and the entropy model (*b*), during slow shoulder flexion trials. The average sum of activation squared model for slow trials (green) is overlaid on results from *in vivo* JRF measurements (*c*) as well as three different models from Nikooyan et al (2010). The symbol (N) designates results are from Nikooyan et al (2010).

5.4. Limitations

A few limitations with EMG and kinematics were found during data collection. One limitation is that this study only used surface EMG and therefore could not collect all of the deep rotator cuff muscles (subscapularis and teres minor), the use of indwelling EMG would have allowed the collection of all muscle activity of the rotator cuff muscles to give more insight into the stabilizing muscles. In order to collect supraspinatus accurately pediatric electrodes were used, but the supraspinatus lies deep to the trapezius.

Studies have shown the possibility of using surface EMG to collect muscle activations of the supraspinatus muscle, but results from this thesis suggest this advice should be used with caution (Allen et al, 2013; Brown et al, 2010). Brown et al (2010) recognized the possibility of picking up signal from the trapezius tendon but neither of the studies collected and compared the two muscles. In order to assess the correlation between the supraspinatus and trapezius muscles for this thesis, the muscle activations were compared for each participant using a cross correlation analysis. The cross correlation revealed an average explained variance (r^2) of 8.0 ±5.0% between supraspinatus and all other muscles collected (except for trapezius) and showed supraspinatus explained 31.6 ±6.0% of the variance in upper trapezius activations, which was significantly higher than all other muscle pair comparisons ($p<0.01$). This shows there may have been cross talk between the two muscles or the muscles may have highly correlated function therefore, another cross correlation was performed between predicted trapezius and predicted supraspinatus activations for comparison. The predicted supraspinatus activations for the sum of squares model (which predicted the least amount of co-activation) were seen to explain 41.4 ± 7.7% of the variance in trapezius. These statistics show that the supraspinatus EMG was activated when the trapezius was active and that this could be attributed to the fact that the muscles have a highly correlated function when lifting the arm in forward flexion.

A limitation affecting the kinematic recording during collection was the number of sensors available for scapular tracking. The Fastrak offers 4 sensors; one was used on the thorax, one on the scapula, and 2 on the arm. The clavicle was not tracked directly as the number of sensors was limited. This limited the kinematics of the clavicle, acromioclavicular (AC) joint, and sternoclavicular (SC) joints seen in the model. The single scapular marker was not sufficient to keep the scapula from crossing into the thorax so a virtual marker was placed on both the trigonum spinae and inferior angle providing better scapular tracking. The virtual markers kept the scapula in a proper orientation, limiting unwanted scapular movement yet still showing upward rotation and posterior tilt during the flexion movements. One scapular marker may have been sufficient if the scapular gliding plane was implemented into the OpenSIM DSEM as stated by Blana et al (2008). The scapular gliding plane is a constraint implemented in the OpenSIM model to constrain the medial border of the scapula to the thorax, but, as seen in this study the scapula would penetrate the thorax proving such a constraint is non-existent in the OpenSIM model. The other major constraint of the DSEM is the glenohumeral JRF constraint which does not allow the joint reaction force to exit the glenoid, theoretically creating a joint which is always stable. It should be noted the stability constraint was not used in this thesis to observe the effects on the stability ratio under different conditions.

OpenSIM has a few limitations itself. The DSEM model in OpenSIM was unable to converge on a solution without help on a majority of trials. An assisted EMG approach (Cholewicki & McGill, 1995; Nikooyan et al, 2012) may have helped, but this limitation was overcome by increasing maximum allowed torque for the model reserve actuators at each joint as seen in previous gait studies (van der Krogt et al, 2012; Steele et al, 2012). The second limitation prevented investigation of movements in the scapular and frontal planes. The DSEM model has 11 degrees of freedom spread over the SC, AC, GH, elbow, and radio-ulnar joints, but it does not have any degrees of freedom between the thorax and the ground. The thorax and ground joint is a weld joint in OpenSIM and, therefore, allows no translation or rotation of the thorax relative to the ground. During collection, the Fastrak base was located in a fixed position next to the Biodex. For each plane of action the arm was kept in approximately the same position (i.e. strapped into the Biodex) relative to the Fastrak base, but the body (thorax) was rotated relative to the Fastrak base in order to place the participant in each plane of action. After markers were normalized to the sternum, and local joint angles were created, the model would not reflect the correct position of the arm relative to the thorax for trials in the scapular and frontal plane. To solve this problem a 6 degree of freedom joint must be created between the thorax and the ground. The most recent version of the Holzbaur et al (2005) model addresses this limitation (Saul et al, 2014).

5.5. Future Directions

Some steps can be taken to increase the accuracy of the current DSEM model. An immediate step would be to create the previously described 6 degree of freedom joint between the thorax and the ground as this would enable thorax rotation and translation to occur. This has very recently been implemented in the newest version of the Holzbaur et al (2005) model called the Upper Extremity Dynamic Model (Saul et al, 2014). Implementing a similar joint in the DSEM increase the accuracy of predictions. Another addition to the model, that could help scapular tracking and, in turn, muscle activity predictions, is the implementation of the scapular gliding plane. Blana et al (2008) have stated it was included in the model but after further investigation it was not actually implemented in the OpenSIM version of the model, which may be due to limitations in the OpenSIM modeling platform.

Overall, when comparing predicted muscle activity to experimental EMG, the sum of activation models explained more variance, and had less RMSD, than the entropy model. The entropy model had a tendency to over-predict the actual muscle activations, but this can be adjusted using the weight factor *W* to decrease the co-contraction portion of the term and lower the predicted muscle activations. Future studies should adjust *W* for different conditions to see if results can explain more variance in experimental values, or look at the effects of other optimization criterion which have been seen to predict co-contraction such as the shift parameter equation (Forster et al, 2004).

As co-activation is considered to be an important factor in the stability of the shoulder anatomically, it is important to take this into consideration when modeling for predicted muscle activations. As seen in this thesis, optimization functions have been used to induce muscular co-activity, but no models have yet minimized the shear force component of the glenohumeral joint reaction force which is the most likely source of why co-contraction occurs at the shoulder. Future implementation of a simple shear minimizing optimization criterion may hold the key to better shoulder model predictions.

5.6. Conclusion

This thesis had three main goals, (i) to compare the performance of several optimization criterion, (ii) investigate co-contraction predicted for each criterion, and (iii) evaluate the predicted joint reaction forces and glenohumeral joint stability. Overall, the predictions from models that minimized the sum of cubed and quartic activations, had significantly higher correlations with experimental EMG than the sum of squares model, and all sum of activation models predicted much better than the entropy model. Significantly more co-activation was predicted as the power of the activation models was raised. A similar trend was seen when comparing the magnitude of joint reaction forces across models, indicating models that predict more co-activation will also predict a larger resultant joint reaction force. Joint reaction forces predicted by all models were highly variable and no significant differences were seen in predicted stability ratios between the models. On average, the glenohumeral joint was predicted to be stable, but the stability of the joint was decreased when the arm was raised above 90°.

This thesis provides a detailed evaluation of several optimization criterion. This evaluation demonstrates which optimization function predicts experimental EMG better in dynamic and static conditions over a large range of motion as well as offers insight into which movements and positions might increase the risk of shoulder instability. Increasing the accuracy of estimates is the most important goal of any musculoskeletal model. By adapting upper extremity models to increase their accuracy, they become more applicable for use by clinicians to assess and improve rehabilitation and surgical techniques, as well as more applicable to future ergonomic tools enabling better proactive shoulder specific job analyses.

REFERENCES

Aalbersberg, S., Kingma, I., Blankevoort, L., & van Dieën, J. H. (2005). Co-contraction during static and dynamic knee extensions in ACL deficient subjects. *Journal of Electromyography and Kinesiology*, *15*(4), 349-357.

Ackland, D. C. & Pandy, M. G. (2009). Lines of action and stabilizing potential of the shoulder musculature. *Journal of Anatomy*, *215*(2), 184-197.

Allen, T. R., Brookham, R. L., Cudlip, A. C., & Dickerson, C. R. (2013). Comparing surface and indwelling electromyographic signals of the supraspinatus and infraspinatus muscles during submaximal axial humeral rotation. *Journal of Electromyography and Kinesiology*, *23*(6), 1343-1349.

Blana, D., Hincapie, J. G., Chadwick, E. K., & Kirsch, R. F. (2008). A musculoskeletal model of the upper extremity for use in the development of neuroprosthetic systems. *Journal of Biomechanics*, *41*(8), 1714-1721.

Bowman, T. G., Hart, J. M., McGuire, B. A., Palmieri, R. M., & Ingersoll, C. D. (2006). A functional fatiguing protocol and deceleration time of the shoulder from an internal rotation perturbation. *Journal of Athletic Training*, *41*(3), 275.

Brown, S. H., Brookham, R. L., & Dickerson, C. R. (2010). High-pass filtering surface EMG in an attempt to better represent the signals detected at the intramuscular level. *Muscle & Nerve*, *41*(2), 234-239.

Cahalan, T. D., Johnson, M. E., & Chao, E. Y. (1991). Shoulder strength analysis using the Cybex II isokinetic dynamometer. *Clinical Orthopaedics and Related Research*, *271*, 249-257.

Carpenter, J. E., Blasier, R. B., & Pellizzon, G. G. (1998). The effects of muscle fatigue on shoulder joint position sense. *The American Journal of Sports Medicine*, *26*(2), 262-265.

Chaffin, D. B. (2005). Improving digital human modelling for proactive ergonomics in design. *Ergonomics*, *48*(5), 478-491.

Charles, S.K. (2012). Matlab Code for shoulder, elbow, and wrist joint angle computation according to ISB recommendations. Manuscript in Preparation.

Cholewicki, J., & McGill, S. M. (1994). EMG assisted optimization: a hybrid approach for estimating muscle forces in an indeterminate biomechanical model. *Journal of Biomechanics*, *27*(10), 1287-1289.

Crowninshield, R. D., & Brand, R. A. (1981). A physiologically based criterion of muscle force prediction in locomotion. *Journal of Biomechanics*, *14*(11), 793-801.

Culham, E., & Peat, M. (1993). Functional anatomy of the shoulder complex. *Journal of Orthopaedic and Sports Physical Therapy*, *18*, 342-342.

Danneskiold-Samsøe, B., Bartels, E. M., Bülow, P. M., Lund, H., Stockmarr, A., Holm, C. C., Watjen, I., Appleyard, M., & Bliddal, H. (2009). Isokinetic and isometric muscle strength in a healthy population with special reference to age and gender. *Acta Physiologica*, *197*(s673), 1-68.

De Groot, J. H., Rozendaal, L. A., Meskers, C. G., & Arwert, H. J. (2004). Isometric shoulder muscle activation patterns for 3-D planar forces: a methodology for musculo-skeletal model validation. *Clinical Biomechanics*, *19*(8), 790-800.

Delp, S. L., & Loan, J. P. (1995). A graphics-based software system to develop and analyze models of musculoskeletal structures. *Computers in Biology and Medicine*, *25*(1), 21-34.

De Luca, C. J., & Forrest, W. J. (1973). Force analysis of individual muscles acting simultaneously on the shoulder joint during isometric abduction. *Journal of Biomechanics*, *6*(4), 385-393.

Dickerson, C. R., Chaffin, D. B., & Hughes, R. E. (2007). A mathematical musculoskeletal shoulder model for proactive ergonomic analysis. *Computer Methods in Biomechanics and Biomedical Engineering*, *10*(6), 389-400

Dubowsky, S. R., Rasmussen, J., Sisto, S. A., & Langrana, N. A. (2008). Validation of a musculoskeletal model of wheelchair propulsion and its application to minimizing shoulder joint forces. *Journal of Biomechanics*, *41*(14), 2981-2988.

Dul, J. (1988). A biomechanical model to quantify shoulder load at the work place. *Clinical Biomechanics*, *3*(3), 124-128.

Dul, J., Townsend, M. A., Shiavi, R., & Johnson, G. E. (1984). Muscular synergism—I. On criteria for load sharing between synergistic muscles. *Journal of Biomechanics*, *17*(9), 663-673.

Erdemir, A., McLean, S., Herzog, W., & van den Bogert, A. J. (2007). Model-based estimation of muscle forces exerted during movements. *Clinical Biomechanics*, *22*(2), 131-154.

FASTRAK Users Manual, Revision C. (2002). Polhemus: Colchester, VT, USA. pg (3-7)

Favre, P., Senteler, M., Hipp, J., Scherrer, S., Gerber, C., & Snedeker, J. G. (2012). An integrated model of active glenohumeral stability. *Journal of biomechanics*, *45*(13), 2248-2255.

Folland, J., Leach, B., Little, T., Hawker, K., Myerson, S., Montgomery, H., & Jones, D. (2000). Angiotensin-converting enzyme genotype affects the response of human skeletal muscle to functional overload. *Experimental Physiology*, *85*(5), 575-579.

Forster, E., Simon, U., Augat, P., & Claes, L. (2004). Extension of a state-of-the-art optimization criterion to predict co-contraction. *Journal of Biomechanics*, *37*(4), 577-581.

Frost, P., & Andersen, J. H. (1999). Shoulder impingement syndrome in relation to shoulder intensive work. *Occupational and Environmental Medicine*, *56*(7), 494-498.

Graichen, H., Stammberger, T., Bonel, H., Englmeier, K. H., Reiser, M., & Eckstein, F. (2000). Glenohumeral translation during active and passive elevation of the shoulder—a 3D open-MRI study. *Journal of biomechanics*, *33*(5), 609-613.

Hodder, J. N., & Keir, P. J. (2013). Obtaining maximum muscle excitation for normalizing shoulder electromyography in dynamic contractions. *Journal of Electromyography and Kinesiology*, *23*(5), 1166-1173.

Högfors, C., Karlsson, D., & Peterson, B. (1995). Structure and internal consistency of a shoulder model. *Journal of Biomechanics*, *28*(7), 767-777.

Högfors, C., Sigholm, G., & Herberts, P. (1987). Biomechanical model of the human shoulder - I. Elements. *Journal of Biomechanics*, *20*(2), 157-166.

Holmes, M. W., & Keir, P. J. (2012). Posture and hand load alter muscular response to sudden lbow perturbations. *Journal of Electromyography and Kinesiology*, *22*(2), 191-198.

Holzbaur, K. R., Murray, W. M., & Delp, S. L. (2005). A model of the upper extremity for simulating musculoskeletal surgery and analyzing neuromuscular control. *Annals of Biomedical Engineering*, *33*(6), 829-840.

Howell, S. M., & Galinat, B. J. (1989). The glenoid-labral socket: a constrained articular surface. *Clinical Orthopaedics and Related Research*, *243*, 122-125.

Hvorslev, C. M. (1927). Studien über die Bewegungen der Schulter. *Skandinavisches Archiv Für Physiologie.* 53, 1-136.

Inman, V. T., & Abbott, L. C. (1944). Observations on the function of the shoulder joint. *The Journal of Bone & Joint Surgery*, *26*(1), 1-30.

Itoi, E., Hsu, H. C., & An, K. N. (1996). Biomechanical investigation of the glenohumeral joint. *Journal of Shoulder and Elbow Surgery*, *5*(5), 407-424.

Jiang, Z., & Mirka, G. A. (2007). Application of an Entropy-Assisted Optimization Model in Prediction of Agonist and Antagonist Muscle Forces. In *Proceedings of the Human Factors and Ergonomics Society Annual Meeting* (Vol. 51, No. 15, pp. 923-927). SAGE Publications.

Karduna, A. R., McClure, P. W., Michener, L. A., & Sennett, B. (2001). Dynamic measurements of three-dimensional scapular kinematics: a validation study. *Journal of Biomechanical Engineering*, *123*(2), 184-190.

Karlsson, D., & Peterson, B. (1992). Towards a model for force predictions in the human shoulder. *Journal of Biomechanics*, *25*(2), 189-199.

Kisiel-Sajewicz, K., Fang, Y., Hrovat, K., Yue, G. H., Siemionow, V., Sun, C. K., Jaskolska, A., Sahgal, V., & Daly, J. J. (2011). Weakening of synergist muscle coupling during reaching movement in stroke patients. *Neurorehabilitation and Neural Repair*, *25*(4), 359-368.

Klein-Breteler, M. D., Spoor, C. W., & Van der Helm, F. C. (1999). Measuring muscle and joint geometry parameters of a shoulder for modeling purposes. *Journal of Biomechanics*, *32*(11), 1191-1197.

Kronberg, M., Nemeth, G., & Brostrom, L. A. (1990). Muscle activity and coordination in the normal shoulder: an electromyographic study. *Clinical Orthopaedics and Related Research*, *257*, 76-85.

Labriola, J. E., Lee, T. Q., Debski, R. E., & McMahon, P. J. (2005). Stability and instability of the glenohumeral joint: the role of shoulder muscles. *Journal of Shoulder and Elbow Surgery*, *14*(1), S32-S38.

Laursen, B., Søgaard, K., & Sjøgaard, G. (2003). Biomechanical model predicting electromyographic activity in three shoulder muscles from 3D kinematics and external forces during cleaning work. *Clinical Biomechanics*, *18*(4), 287-295.

Lee, S. B., Kim, K. J., O'Driscoll, S. W., Morrey, B. F., & An, K. N. (2000). Dynamic Glenohumeral Stability provided by the rotator cuff muscles in the mid-range and end-range of motion a study in cadavera. *The Journal of Bone & Joint Surgery*, *82*(6), 849-849.

Lewek, M. D., Rudolph, K. S., & Snyder-Mackler, L. (2004). Control of frontal plane knee laxity during gait in patients with medial compartment knee osteoarthritis. *Osteoarthritis and Cartilage*, *12*(9), 745-751.

Liu, M. M., Herzog, W., & Savelberg, H. H. (1999). Dynamic muscle force predictions from EMG: an artificial neural network approach. *Journal of Electromyography and Kinesiology*, *9*(6), 391-400.

Lippitt, S., & Matsen, F. (1993). Mechanisms of glenohumeral joint stability. *Clinical Orthopaedics and Related Research*, *291*, 20-28.

Lippitt, S. B., Vanderhooft, J. E., Harris, S. L., Sidles, J. A., Harryman II, D. T., &Matsen III, F. A. (1993). Glenohumeral stability from concavity-compression: a quantitative analysis. *Journal of Shoulder and Elbow Surgery*, *2*(1), 27-35.

Lo, I. K., Nonweiler, B., Woolfrey, M., Litchfield, R., & Kirkley, A. (2004). An evaluation of the apprehension, relocation, and surprise tests for anterior shoulder instability. *The American Journal of Sports Medicine*, *32*(2), 301-307.

Ludewig, P. M., & Cook, T. M. (2000). Alterations in shoulder kinematics and associated muscle activity in people with symptoms of shoulder impingement. *Physical Therapy*, *80*(3), 276-291.

Macintosh, A. (2014). An open-source musculoskeletal model and EMG-constrained static optimization solution method to predict co-contraction in the index finger. Master of Science Thesis: McMaster University, ON, Canada.

Magermans, D. J., Chadwick, E. K. J., Veeger, H. E. J., Rozing, P. M., & Van der Helm, F. C. T. (2004). Effectiveness of tendon transfers for massive rotator cuff tears: a simulation study. *Clinical Biomechanics*, *19*(2), 116-122.

McClure, P. W., Michener, L. A., Sennett, B. J., & Karduna, A. R. (2001). Direct 3-dimensional measurement of scapular kinematics during dynamic movements in vivo. *Journal of Shoulder and Elbow Surgery*, *10*(3), 269-277.

McQuade, K. J., & Smidt, G. L. (1998). Dynamic scapulohumeral rhythm: the effects of external resistance during elevation of the arm in the scapular plane. *Journal of Orthopaedic & Sports Physical Therapy*, *27*(2), 125-133.

Minekus, J. (1997). "Kinematical model of the human elbow". M.Sc Thesis: Delft University of Technology.

Mollier, S. (1899). Ueber die Statik und Mechanik des menslichen Schultergurtels unter normalen und pathologishcen Verhaltnissen. Festschr. F. C. v. Kupfeer, Jena.

Morrison, D. S., Greenbaum, B. S., & Einhorn, A. (2000). Shoulder impingement. *Orthopedic Clinics of North America*, *31*(2), 285-293.

Morrow, M., Kaufman, K. R., & An, K. N. (2010). Shoulder model validation and joint contact forces during wheelchair activities. *Journal of Biomechanics*, *43*(13), 2487-2492.

Nikooyan, A. A., Veeger, H. E. J., Chadwick, E. K. J., Praagman, M., & van der Helm, F. C. (2011). Development of a comprehensive musculoskeletal model of the shoulder and elbow. *Medical & Biological Engineering & Computing*, *49*(12), 1425-1435.

Nikooyan, A. A., Veeger, H., Westerhoff, P., Bergmann, G., & Van der Helm, F. C. (2013). Relative Contribution of Different Muscle Energy Consumption Processes in an Energy-Based Muscle Load Sharing Cost Function. *Journal of Mechanics in Medicine and Biology*, *13*(01).

Nikooyan, A. A., Veeger, H. E. J., Westerhoff, P., Bolsterlee, B., Graichen, F., Bergmann, G., & Van der Helm, F. C. T. (2012). An EMG-driven musculoskeletal model of the shoulder. *Human Movement Science*, *31*(2), 429-447.

Nikooyan, A. A., Veeger, H. E. J., Westerhoff, P., Graichen, F., Bergmann, G., & Van Der Helm, F. C. T. (2010). Validation of the Delft Shoulder and Elbow Model using in-vivo glenohumeral joint contact forces. *Journal of Biomechanics*, *43*(15), 3007-3014.

Pedotti, A., Krishnan, V. V., & Stark, L. (1978). Optimization of muscle-force sequencing in human locomotion. *Mathematical Biosciences*, *38*(1), 57-76.

Perotto, A., & Delagi, E. F. (2005). *Anatomical guide for the electromyographer: the limbs and trunk*. Charles C Thomas Publisher, Springfield, Illinois.

Poppen, N. K., & Walker, P. S. (1978). Forces at the glenohumeral joint in abduction. *Clinical Orthopaedics and Related Research*, *135*, 165-170.

Praagman, M., Chadwick, E. K. J., Van Der Helm, F. C. T., & Veeger, H. E. J. (2006). The relationship between two different mechanical cost functions and muscle oxygen consumption. *Journal of Biomechanics*, *39*(4), 758-765.

Raikova, R. T., & Prilutsky, B. I. (2001). Sensitivity of predicted muscle forces to parameters of the optimization-based human leg model revealed by analytical and numerical analyses. *Journal of Biomechanics*, *34*(10), 1243-1255.

Saha, A. K. (1971). Dynamic stability of the glenohumeral joint. *Acta Orthopaedica*, *42*(6), 491-505.

Saul, K. R., Hu, X., Goehler, C. M., Vidt, M. E., Daly, M., Velisar, A., & Murray, W. M. (2014). Benchmarking of dynamic simulation predictions in two software platforms using an upper limb musculoskeletal model. *Computer Methods in Biomechanics and Biomedical Engineering*, (ahead-of-print), 1-14.

Shiino, K. (1913). Schultergelenkbewegungen und Schultermuskelarbeit. *Archives of Anatomy and Physiology.* (Supple. Anat. Abtig) 1-88.

Steele, K. M., van der Krogt, M. M., Schwartz, M. H., & Delp, S. L. (2012). How much muscle strength is required to walk in a crouch gait?. *Journal of Biomechanics*, *45*(15), 2564-2569.

Steenbrink, F., De Groot, J. H., Veeger, H. E. J., van der Helm, F. C. T., & Rozing, P. M. (2009). Glenohumeral stability in simulated rotator cuff tears. *Journal of Biomechanics*, *42*(11), 1740-1745.

Svendsen, S. W., Bonde, J. P., Mathiassen, S. E., Stengaard-Pedersen, K., & Frich, L. H. (2004). Work related shoulder disorders: quantitative exposure-response relations with reference to arm posture. *Occupational and Environmental Medicine*, *61*(10), 844-853.

Szucs, K., Navalgund, A., & Borstad, J. D. (2009). Scapular muscle activation and co-activation following a fatigue task. *Medical & Biological Engineering & Computing*, *47*(5), 487-495.

Terrier, A., Vogel, A., Capezzali, M., & Farron, A. (2008). An algorithm to allow humerus translation in the indeterminate problem of shoulder abduction. *Medical Engineering & Physics*, *30*(6), 710-716.

Van der Helm, F. C. (1994a). A finite element musculoskeletal model of the shoulder mechanism. *Journal of Biomechanics*, *27*(5), 551-569.

Van der Helm, F. C. (1994b). Analysis of the kinematic and dynamic behavior of the shoulder mechanism. *Journal of Biomechanics*, *27*(5), 527-550.

van der Krogt, M. M., Delp, S. L., & Schwartz, M. H. (2012). How robust is human gait to muscle weakness?. *Gait & Posture*, *36*(1), 113-119.

Veeger, H. E. J., Rozendaal, L. A., & Van Der Helm, F. C. T. (2002). Load on the shoulder in low intensity wheelchair propulsion. *Clinical Biomechanics*, *17*(3), 211-218.

Veeger, H. E. J., & Van Der Helm, F. C. T. (2007). Shoulder function: the perfect compromise between mobility and stability. *Journal of Biomechanics*, *40*(10), 2119-2129.

Von Schroeder, H. P., Kuiper, S. D., & Botte, M. J. (2001). Osseous anatomy of the scapula. *Clinical Orthopaedics and Related Research*, *383*, 131-139.

Waite, D. L., Brookham, R. L., & Dickerson, C. R. (2010). On the suitability of using surface electrode placements to estimate muscle activity of the rotator cuff as recorded by intramuscular electrodes. *Journal of Electromyography and Kinesiology*, *20*(5), 903-911.

Warner, J. J., Micheli, L. J., Arslanian, L. E., Kennedy, J., & Kennedy, R. (1990). Patterns of flexibility, laxity, and strength in normal shoulders and shoulders with instability and impingement. *The American Journal of Sports Medicine*, *18*(4), 366-375.

Wattanaprakornkul, D., Cathers, I., Halaki, M., & Ginn, K. A. (2011). The rotator cuff muscles have a direction specific recruitment pattern during shoulder flexion and extension exercises. *Journal of Science and Medicine in Sport*, *14*(5), 376-382.

Winter, D.A. (1990). Biomechanics and Motor Control of Human Movement. 2nd edition. John Wiley & Sons, Inc, Toronto, 1990.

Workplace Safety and Insurance Board. (2011). High Impact Claims – Fact Sheet. Ontario, Canada.

Workplace Safety and Insurance Board. (2013). By the Numbers: WSIB Statistical Report. Ontario, Canada.

Wu, G., Van Der Helm, F. C., Veeger, H. E. J., Makhsous, M., Van Roy, P., Anglin, C., Nagels, J., Karduna, A.R., McQuade, K., Wang, X., Werner, F.W., & Buchholz, B. (2005). ISB recommendation on definitions of joint coordinate systems of various joints for the reporting of human joint motion—Part II: shoulder, elbow, wrist and hand. *Journal of Biomechanics*, *38*(5), 981-992.

Yamamoto, A., Takagishi, K., Osawa, T., Yanagawa, T., Nakajima, D., Shitara, H., & Kobayashi, T. (2010). Prevalence and risk factors of a rotator cuff tear in the general population. *Journal of Shoulder and Elbow Surgery*, *19*(1), 116-120.

Yanagawa, T., Goodwin, C. J., Shelburne, K. B., Giphart, J. E., Torry, M. R., & Pandy, M. G. (2008). Contributions of the individual muscles of the shoulder to glenohumeral joint stability during abduction. *Journal of Biomechanical Engineering*, *130*(2), 21024-21024.

APPENDIX A

Mean normalized EMG shown as a percent of maximum for all eight muscles under each condition in each plane. Standard deviations for each mean are shown in the table below.

	Sagittal Plane (Flexion)								
	Static 60°				Static 120°				Stress test
MEANS	Low Force		High Force		Low Force		High Force		N/A
Muscle	Low arm	Upper arm	Low arm	Upper arm	Low arm	Upper arm	Low arm	Upper arm	N/A
Lats.	2.231	5.608	2.435	5.912	4.380	10.581	4.659	10.363	10.102
Infra.	6.052	26.266	5.886	18.533	7.406	32.241	7.330	29.744	33.092
Upper Traps	7.067	18.373	5.908	16.593	12.536	41.176	12.766	42.423	27.313
Supra.	13.823	31.594	11.183	28.478	20.308	48.625	19.914	54.767	43.958
Post. Delt.	2.128	6.371	1.978	5.705	3.627	12.444	2.903	13.055	49.852
Mid. Delt.	8.172	24.991	8.211	23.591	13.536	34.745	14.089	38.965	44.495
Ant. Delt.	12.816	37.921	12.617	36.405	15.407	39.664	19.390	47.264	9.870
Pec. Major	3.289	8.393	3.808	11.071	2.237	5.597	3.113	9.873	4.169
Standard Deviation									
Lats.	1.591	3.250	1.718	3.991	2.899	5.340	4.089	5.473	4.362
Infra.	6.639	6.020	10.333	8.781	6.594	17.802	10.429	22.437	12.078
Upper Traps	3.296	9.372	3.532	5.707	6.246	18.711	8.632	18.017	10.348
Supra.	5.165	13.417	4.785	10.289	7.145	13.354	8.604	17.985	13.472
Post. Delt.	0.892	3.100	1.485	2.751	1.823	7.061	1.303	7.957	9.550
Mid. Delt.	2.187	6.420	2.750	6.925	4.872	10.102	4.884	11.360	13.059
Ant. Delt.	3.963	10.720	4.379	8.790	5.748	10.647	8.979	14.043	4.980
Pec. Major	3.075	8.195	3.679	8.354	2.123	4.487	3.549	11.365	3.850

	Sagittal Plane (Flexion)															
	Fast Dynamic (60°/sec)															
	Low Torque (10 Nm)								High Torque (35 Nm)							
MEANS	Low arm (point of force application)				Upper arm (point of force application)				Low arm				Upper arm			
Muscle	**30°**	**60°**	**90°**	**120°**	**30°**	**60°**	**90°**	**120°**	**30°**	**60°**	**90°**	**120°**	**30°**	**60°**	**90°**	**120°**
Lats.	2.705	3.765	5.736	5.771	2.243	3.494	5.928	5.944	3.472	4.717	7.005	7.822	4.664	6.210	7.666	7.179
Infra.	12.278	17.600	19.530	15.619	9.793	11.882	15.117	11.784	20.883	32.310	51.141	44.529	22.659	32.738	34.026	32.892
Upper Traps	10.468	19.379	30.801	22.706	6.479	12.439	24.431	15.368	19.671	33.574	58.593	41.170	16.053	34.214	47.736	38.121
Supra.	16.994	26.762	33.667	24.692	14.187	23.814	29.810	23.266	27.733	43.109	61.620	49.530	24.145	41.972	52.288	44.881
Post Delt.	2.652	3.798	5.275	4.986	2.479	3.266	4.374	3.740	4.696	6.720	11.291	11.479	5.332	6.757	10.107	9.519
Mid Delt.	13.122	16.362	23.105	18.668	11.023	15.103	26.749	18.449	26.869	28.727	37.514	29.740	25.552	31.226	35.864	29.337
Ant Delt.	29.812	32.909	34.654	24.741	24.424	30.546	42.221	31.733	48.001	51.264	55.315	46.572	47.895	51.727	55.890	44.554
Pec Major	9.414	6.468	5.606	5.432	8.740	6.707	6.212	6.182	20.834	14.497	11.757	8.966	25.496	15.965	12.152	9.147
Standard Deviations																
Lats.	2.826	2.867	4.104	2.710	1.917	2.418	4.306	5.228	2.642	3.185	3.896	5.448	2.979	3.794	3.941	4.602
Infra.	12.199	12.231	11.364	11.265	12.878	11.349	10.872	11.678	13.352	13.038	18.484	17.337	15.218	13.886	14.339	17.514
Upper Traps	6.342	8.680	21.495	17.125	3.508	5.002	12.858	13.166	6.413	14.752	27.928	16.969	8.710	13.676	15.878	18.748
Supra.	6.322	6.518	16.194	17.724	7.252	10.565	11.284	19.092	14.248	15.850	13.742	14.239	9.925	14.644	10.070	17.043
Post Delt.	1.561	1.738	2.059	2.952	1.485	1.783	1.826	2.257	2.064	3.961	8.226	11.360	2.729	3.031	6.622	6.843
Mid Delt.	6.678	5.234	11.852	12.282	5.671	6.430	11.312	11.806	7.771	11.142	10.308	8.148	10.155	8.508	4.863	13.959
Ant Delt.	20.043	17.822	16.943	17.528	14.915	17.669	15.889	23.335	16.005	16.040	15.256	16.226	15.640	12.276	17.251	21.668
Pec Major	7.348	5.838	5.420	4.748	4.997	5.866	5.214	6.409	12.458	11.055	11.421	11.185	14.316	10.782	11.899	9.306

	Sagittal Plane (Flexion)															
	Slow Dynamic (120°/sec)															
	Low Torque (10 Nm)								High Torque (35 Nm)							
MEANS	Low arm				Upper arm				Low arm				Upper arm			
Muscle	**30°**	**60°**	**90°**	**120°**	**30°**	**60°**	**90°**	**120°**	**30°**	**60°**	**90°**	**120°**	**30°**	**60°**	**90°**	**120°**
Lats.	1.553	2.848	5.008	7.837	1.578	3.391	5.361	5.798	3.015	6.137	8.683	9.650	4.119	6.822	9.429	7.994
Infra.	6.777	10.712	13.914	20.645	7.390	8.913	11.652	11.690	14.334	32.168	48.818	45.930	18.033	29.771	35.982	30.759
Upper Traps	6.342	13.229	23.362	26.729	4.721	9.774	21.704	22.732	11.253	24.519	47.879	44.516	11.328	33.359	49.684	39.462
Supra.	12.673	19.552	28.151	30.984	13.132	19.357	31.023	29.218	20.417	34.294	54.907	47.598	22.429	46.783	59.323	44.018
Post Delt.	1.878	3.108	4.772	6.796	1.786	2.644	5.111	5.027	3.587	5.954	10.464	13.446	4.863	8.589	12.682	9.330
Mid Delt.	7.845	12.693	23.364	26.626	7.828	14.037	26.861	24.339	15.123	25.537	33.667	30.509	23.851	33.159	40.753	34.062
Ant Delt.	16.430	23.292	34.386	36.138	14.968	22.690	37.826	33.177	34.324	46.318	52.197	45.018	39.285	51.089	55.323	40.623
Pec Major	5.555	4.435	4.881	5.853	5.840	4.028	6.138	4.092	16.668	14.345	10.700	8.135	20.505	13.200	10.515	6.002
Standard Deviations																
Lats.	1.644	2.154	3.887	5.503	1.437	3.371	4.880	3.491	2.699	4.623	4.913	5.549	3.275	4.129	4.252	4.716
Infra.	10.040	10.054	10.108	11.707	11.316	10.952	10.939	11.610	10.031	14.108	21.766	18.704	10.941	16.911	13.071	15.485
Upper Traps	3.124	6.681	15.123	15.066	3.249	3.844	9.721	11.992	4.964	9.970	17.214	17.901	5.217	13.106	16.686	21.911
Supra.	6.460	8.177	12.567	14.388	6.994	7.643	12.206	13.887	11.320	13.326	10.451	11.921	14.590	20.620	20.096	17.511
Post Delt.	1.392	2.320	2.980	4.396	1.084	1.269	2.836	2.860	2.106	3.306	7.139	13.365	3.331	6.989	8.664	5.690
Mid Delt.	5.080	6.600	8.527	10.879	3.450	6.957	12.642	10.699	5.367	6.962	7.423	8.751	6.500	10.549	9.700	14.189
Ant Delt.	11.194	16.106	14.107	12.893	8.534	14.221	15.278	13.650	18.834	16.469	9.869	12.002	13.777	17.040	15.601	25.079
Pec Major	5.999	4.391	5.366	7.906	5.016	4.934	8.684	2.906	14.734	13.747	11.277	9.959	13.539	12.530	10.483	3.998

	Scapular Plane (Flexion)															
	Fast Dynamic (60°/sec)															
	Low Torque (10 Nm)								High Torque (35 Nm)							
MEANS	Low arm				Upper arm				Low arm				Upper arm			
Muscle	30°	60°	90°	120°	30°	60°	90°	120°	30°	60°	90°	120°	30°	60°	90°	120°
Lats.	1.892	2.830	5.820	6.396	2.542	2.885	5.602	5.977	3.103	4.421	7.017	8.681	3.675	5.975	8.145	6.002
Infra.	10.342	11.875	18.106	12.948	10.107	10.870	13.828	9.303	28.905	38.075	44.427	35.600	22.410	35.743	35.723	22.563
Upper Traps	11.281	16.247	27.933	21.689	10.867	17.461	29.461	14.157	25.118	39.149	48.900	40.407	22.479	36.539	53.565	28.217
Supra.	19.409	23.427	31.642	24.116	19.127	26.393	38.067	20.530	32.520	49.049	61.659	42.184	31.421	49.185	63.122	31.541
Post Delt.	2.913	3.658	5.625	4.292	3.234	4.346	5.963	4.030	7.094	8.828	13.230	11.294	6.217	10.611	15.505	9.478
Mid Delt.	15.402	18.203	28.771	20.804	19.176	22.558	30.819	17.596	32.314	35.548	43.130	33.002	32.356	38.958	43.823	29.376
Ant Delt.	23.334	26.307	39.517	26.151	25.502	31.571	43.575	23.340	47.477	52.196	60.924	44.408	51.797	57.768	61.511	37.328
Pec Major	3.142	3.425	4.294	4.171	3.249	3.182	4.576	4.132	7.450	6.916	7.281	8.914	8.896	8.638	10.545	7.124
Standard Deviations																
Lats.	1.259	1.865	3.022	4.196	2.429	1.866	3.210	4.705	2.133	2.565	3.912	5.127	3.207	3.909	4.589	4.395
Infra.	10.174	9.576	9.051	9.612	9.628	8.840	8.296	8.181	17.668	19.021	25.139	14.716	11.680	24.646	22.325	9.415
Upper Traps	3.859	4.525	14.187	16.166	4.889	6.878	14.374	6.980	11.664	11.683	15.687	19.154	7.574	13.975	25.435	13.993
Supra.	6.296	5.756	14.605	17.008	7.371	8.762	14.844	12.726	9.706	12.962	19.824	22.789	10.969	19.807	25.048	14.327
Post Delt.	2.188	1.672	2.146	1.901	2.244	2.418	3.018	1.996	5.279	5.620	7.522	9.610	5.645	9.745	13.032	9.985
Mid Delt.	6.699	3.447	11.250	10.995	9.247	8.973	12.053	10.893	7.150	7.853	7.407	17.083	10.989	12.614	8.486	14.316
Ant Delt.	10.838	9.638	21.557	11.678	9.359	12.886	17.800	17.418	16.653	17.847	11.978	25.276	18.800	19.561	14.807	15.629
Pec Major	2.221	3.188	2.938	2.867	1.547	1.726	3.204	3.372	4.540	4.450	6.715	7.258	7.378	5.443	9.419	8.535

	Scapular Plane (Flexion)															
	Slow Dynamic (120°/sec)															
	Low Torque (10 Nm)								High Torque (35 Nm)							
MEANS	Low arm				Upper arm				Low arm				Upper arm			
Muscle	30°	60°	90°	120°	30°	60°	90°	120°	30°	60°	90°	120°	30°	60°	90°	120°
Lats.	1.689	2.741	4.275	7.037	1.625	3.298	4.720	6.450	3.226	5.606	7.894	8.538	3.402	5.508	8.515	7.501
Infra.	6.820	10.981	12.323	15.833	6.983	8.725	9.748	10.347	18.560	35.207	39.713	43.038	17.934	25.219	29.891	22.324
Upper Traps	9.292	16.018	20.410	27.751	8.195	12.047	16.873	25.829	16.702	32.048	45.937	48.093	17.300	28.789	46.036	37.642
Supra.	15.870	21.947	27.672	33.616	14.620	19.458	25.403	31.780	28.191	45.804	55.143	54.422	24.618	40.671	59.362	41.034
Post Delt.	1.907	3.486	5.159	7.373	1.953	3.051	4.205	6.027	5.193	9.349	12.223	14.665	5.915	8.577	12.733	10.079
Mid Delt.	10.554	16.202	26.641	35.561	10.259	15.999	22.163	29.879	25.265	33.633	41.778	38.765	31.059	34.818	44.519	31.051
Ant Delt.	16.323	20.303	28.392	34.736	16.787	21.337	31.424	42.173	39.450	45.725	50.130	51.111	43.786	45.862	58.346	38.674
Pec Major	2.659	2.969	3.209	4.330	2.524	3.237	3.628	4.701	7.539	6.966	7.562	8.457	6.592	5.874	7.692	6.050
Standard Deviations																
Lats.	1.748	2.693	3.488	5.645	1.600	3.022	4.552	5.141	3.191	4.622	4.424	4.869	1.946	2.900	4.688	5.475
Infra.	10.958	10.551	10.101	9.534	11.371	10.824	11.234	9.699	10.452	12.769	21.915	16.590	11.501	15.119	17.564	14.420
Upper Traps	4.375	9.335	9.448	8.622	6.101	5.873	9.411	10.906	6.215	13.272	18.368	13.254	6.880	10.863	15.795	17.549
Supra.	6.658	8.237	10.008	10.241	7.113	8.869	12.174	14.018	11.253	18.219	18.582	19.789	8.891	18.072	24.577	24.960
Post Delt.	1.269	2.252	3.601	3.891	1.363	1.375	2.241	2.640	3.711	6.696	8.135	10.966	2.879	5.675	9.647	6.761
Mid Delt.	3.346	5.176	11.490	10.921	4.256	6.447	8.059	11.222	6.916	6.094	8.474	4.846	9.236	10.416	11.111	13.032
Ant Delt.	11.225	12.713	16.417	10.309	10.360	9.172	12.134	14.702	19.605	19.034	14.619	13.706	15.401	15.774	16.796	17.201
Pec Major	2.614	3.534	3.414	4.135	1.986	3.006	3.504	4.222	5.982	6.651	7.646	10.318	4.223	4.706	6.053	5.199

	Frontal Plane (Abduction)															
	Fast Dynamic (60°/sec)															
	Low Force								High Force							
MEANS	Low arm				Upper arm				Low arm				Upper arm			
muscle	**30°**	**60°**	**90°**	**120°**	**30°**	**60°**	**90°**	**120°**	**30°**	**60°**	**90°**	**120°**	**30°**	**60°**	**90°**	**120°**
Lats.	2.300	3.708	6.146	6.803	2.016	3.410	5.668	3.802	3.262	5.137	6.273	5.494	5.029	6.291	6.281	6.328
Infra.	10.040	11.223	16.425	10.024	6.946	7.574	9.368	5.424	25.829	28.452	32.570	22.729	20.963	27.327	31.984	20.996
Upper Traps	15.913	21.865	34.052	18.662	15.517	23.852	37.032	11.566	26.640	43.064	52.173	37.315	33.090	50.723	59.157	33.086
Supra.	24.073	28.510	39.685	18.308	20.899	28.789	39.605	13.936	31.251	52.366	56.650	35.570	40.917	58.072	58.696	35.081
Post Delt.	4.187	6.715	9.526	5.613	4.494	6.623	9.148	4.757	10.358	11.471	11.192	7.267	12.033	16.624	16.600	13.057
Mid Delt.	23.284	28.669	36.296	19.593	28.006	28.973	39.377	16.106	41.099	39.903	41.721	25.615	46.140	53.502	50.852	31.138
Ant Delt.	27.611	31.027	42.676	23.534	30.906	30.764	44.774	17.404	48.098	55.180	54.129	35.822	49.796	62.432	63.836	42.257
Pec Major	3.266	3.914	4.775	5.251	2.838	3.371	3.762	3.224	5.187	4.955	5.819	5.035	5.049	6.083	6.350	5.416
Standard Deviations																
Lats.	1.778	3.409	5.855	5.744	1.355	2.542	4.222	2.332	1.851	3.200	3.463	4.342	3.951	3.461	3.800	5.171
Infra.	7.037	6.155	8.478	8.001	5.735	3.982	4.977	4.676	14.309	12.489	16.978	12.660	10.619	8.908	9.535	9.501
Upper Traps	6.420	9.165	12.513	17.644	4.132	6.888	12.880	6.887	7.409	15.038	17.669	26.789	10.008	12.268	16.969	14.501
Supra.	8.903	10.096	15.667	13.462	5.822	8.017	11.375	7.758	8.472	18.344	17.778	25.087	13.534	14.008	16.429	18.580
Post Delt.	2.076	5.085	6.222	2.285	2.250	4.807	6.207	2.317	4.912	5.412	6.202	4.890	7.388	11.076	10.509	10.866
Mid Delt.	5.694	8.071	10.259	15.479	7.515	7.169	8.159	11.375	7.215	8.953	9.671	15.089	8.782	9.267	9.964	10.309
Ant Delt.	11.281	18.568	13.448	17.237	13.129	14.478	7.162	15.675	22.386	17.833	16.994	21.391	17.430	13.783	14.876	14.429
Pec Major	3.484	4.864	4.351	4.309	2.706	3.879	2.732	2.466	4.712	4.421	4.555	4.563	4.124	4.407	4.381	5.056

	Frontal Plane (Abduction)															
	Slow Dynamic (120°/sec)															
	Low Torque (10 Nm)								High Torque (35 Nm)							
MEANS	Low arm				Upper arm				Low arm				Upper arm			
Muscle	**30°**	**60°**	**90°**	**120°**	**30°**	**60°**	**90°**	**120°**	**30°**	**60°**	**90°**	**120°**	**30°**	**60°**	**90°**	**120°**
Lats.	2.744	3.522	4.441	5.137	2.396	3.312	4.810	5.779	2.804	4.463	6.419	8.720	4.014	6.146	8.578	8.598
Infra.	6.197	8.042	10.970	12.198	6.469	8.693	9.553	9.729	15.352	22.171	25.678	28.187	16.486	26.741	25.091	21.554
Upper Traps	10.422	15.933	20.739	28.196	9.755	15.123	19.283	22.271	19.041	33.056	45.552	51.529	23.711	41.528	49.947	37.450
Supra.	17.005	23.074	25.502	30.494	15.579	22.362	27.157	29.987	26.498	43.346	47.013	48.474	31.547	50.602	53.500	39.605
Post Delt.	3.436	4.897	5.455	5.912	2.542	4.067	4.768	6.424	7.306	9.992	10.388	10.892	8.693	11.846	13.531	12.431
Mid Delt.	15.017	21.394	26.649	33.020	14.125	20.761	27.403	32.944	33.556	38.903	40.516	38.538	41.256	46.180	47.361	39.107
Ant Delt.	14.116	19.380	25.165	35.938	15.282	21.419	30.521	35.039	35.539	43.588	49.169	61.506	47.351	54.944	58.232	46.379
Pec Major	1.955	2.512	3.088	3.925	2.005	2.561	3.151	3.891	4.407	5.425	6.297	8.428	4.919	5.827	6.967	7.261
Standard Deviations																
Lats.	4.870	4.499	4.385	3.916	2.852	3.016	3.731	4.671	3.064	3.236	4.168	7.294	3.306	3.969	5.701	6.562
Infra.	9.974	9.308	10.481	10.658	10.881	11.060	10.504	9.684	9.889	11.594	10.926	17.042	10.148	9.789	12.074	12.357
Upper Traps	4.890	6.068	10.902	15.418	5.254	5.408	8.703	10.953	7.598	8.969	12.590	20.232	9.660	12.768	22.801	17.919
Supra.	7.353	6.947	9.145	12.056	4.935	7.726	11.090	12.365	12.522	13.775	11.181	16.344	9.430	12.501	16.927	11.507
Post Delt.	2.169	2.883	3.252	2.713	1.265	2.265	2.574	3.103	5.091	6.076	6.714	9.079	5.156	7.831	7.945	11.756
Mid Delt.	5.622	7.851	9.241	10.540	7.496	8.324	7.328	13.039	12.263	9.665	9.999	16.728	6.863	8.263	9.924	10.972
Ant Delt.	8.778	11.835	9.989	8.244	6.577	8.925	14.416	11.370	19.011	14.002	9.278	27.310	17.231	12.445	11.998	13.148
Pec Major	2.216	2.920	3.302	2.377	1.796	2.363	2.888	3.260	5.544	5.545	5.764	10.110	4.745	5.168	5.644	6.504

APPENDIX B

McMaster University
Inspiring Innovation and Discovery

McMaster University Research Ethics Board (MREB)

c/o Research Office for Administrative Development and Support, MREB Secretariat, GH-305/H, e-mail: ethicsoffice@mcmaster.ca

CERTIFICATE OF ETHICS CLEARANCE TO INVOLVE HUMAN PARTICIPANTS IN RESEARCH

Application Status: ☐ **New** ☑ **Addendum | Project Number:** 2013 012

TITLE OF RESEARCH PROJECT:

Investigating methods of shoulder strength testing and their ability to accurately predict functional arm strength: Sub Protocol - Dynamic and Static Shoulder Strength Relationship

Faculty Investigator(s)/ Supervisor(s)	Dept./Address	Phone	E-Mail
J. Hodder	Kinesiology	20175	hodderjn@mcmaster.ca

Co-Investigator(s):

J. Potvin, P. Keir

Student Investigator(s)	Dept./Address	Phone	E-Mail
S. Savoie	Kinesiology	20175	savoiesm@mcmaster.ca

Co-Investigator(s):

A. McDonald

The application in support of the above research project has been reviewed by the MREB to ensure compliance with the Tri-Council Policy Statement and the McMaster University Policies and Guidelines for Research Involving Human Participants. The following ethics certification is provided by the MREB:

☐ The application protocol is cleared as presented without questions or requests for modification.

☑ The application protocol is cleared as revised without questions or requests for modification.

☐ The application protocol is cleared subject to clarification and/or modification as appended or identified below:

COMMENTS AND CONDITIONS: Ongoing clearance is contingent on completing the annual completed/status report. A "Change Request" or amendment must be made and cleared before any alterations are made to the research.

Amendment#2, cleared April 16, 2014

Reporting Frequency: **Annual:** Mar-21-2015 **Other:**

Date: Mar-21-2013 **Acting Chair, Dr. D. Pawluch**

APPENDIX C

April 14, 2014

LETTER OF INFORMATION / CONSENT

Investigating methods of shoulder strength testing and their ability to accurately predict functional arm strength

Investigators:

Principal Investigators:

Dr. Peter Keir	Spencer Savoie	Alison Mcdonald
Department of Kinesiology	Department of Kinesiology	Department of Kinesiology
McMaster University	McMaster University	McMaster University
Hamilton, Ontario, Canada	Hamilton, Ontario, Canada	Hamilton, Ontario, Canada
(905) 525-9140 ext. 23543	**(905) 525-9140 ext.20175**	**(905) 525-9140 ext. 20175**
pjkeir@mcmaster.ca	savoiesm@mcmaster.ca	mcdonaac@mcmaster.ca

Research Sponsor: **Automotive Partnership Canada**

Purpose of the Study

The purpose of this study is to measure shoulder strength, motion, and the associated muscle activity for a variety of upper body movements and postures to use as input and validation for an upper extremity musculoskeletal model.

You are being invited to participate in a research study conducted by Spencer Savoie (M.Sc. candidate) because you are a healthy male from the Hamilton community or McMaster University population. The study will help the investigators to build a database of shoulder strength and muscle activity for a variety of motions and postures. The data from this study will be incorporated into models that will allow us to more accurately predict the strength capabilities of workers. The model can then be used to determine if the strength requirements of various upper extremity workplace tasks are within the capabilities of the workers with a goal of reducing the risk of workplace injury.

In order to decide whether or not you want to be a part of this research study, you should understand what is involved and the potential risks and benefits. This form gives detailed information about the research study, which will be discussed with you. Once you clearly understand the study, you will be asked to sign this form if you wish to participate. Please take your time to make your decision. Feel free to discuss it with your friends and family.

Procedures involved in the Research

In this study, we are interested in static and dynamic shoulder strength as well as muscle activity in various postures explained below. You will be asked to perform maximal and submaximal static and dynamic shoulder exertions while seated in a piece of equipment called a Biodex. The Biodex is an isokinetic dynamometer, this means it can measure the force applied against it while it is still or moving at a constant velocity. This piece of equipment is not dissimilar to some of the pieces of equipment that can be found in a gym to strengthen the upper body except the speed is controlled. Each trial will consist of a specific upper body movement as seen in Table 1. Trials are short (5-30 seconds) and you will have sufficient time to rest between trials. Electromyography (EMG) and arm motion will be collected. EMG records the activation of muscles by placing electrodes on the skin over the muscle belly. Motion is recorded by placing sensors on the skin which will give their relative position, roll, pitch, and yaw based on the distance from a small electromagnetic base. The duration of the study is one 3 hour session.

Table 1: Movement descriptions

Plane	Action	Description
0 degrees (sagittal plane)	Flexion	Arm raise with arm forward
	Extension	Arm lowering with arm forward
30 degrees (scapular plane)	Flexion	Arm raise with arm to the side
	Extension	Arm lowering with arm to the side
90 degrees (frontal plane)	Abduction	Arm raise with arm to the side
	Adduction	Arm lowering with arm to the side
	External rotation	Rotating arm away from body (clockwise for right arm)
	Internal Rotation	Rotating arm towards body (counter-clockwise for right arm)

Figure 1: Biodex apparatus with shoulder attachment, participant is in 90 degree plane (sagittal) performing arm flexion (left). Participant is performing external rotation (right).

Potential Harms, Risks or Discomforts:
It is not possible to predict all possible risks or discomforts that participants may experience in any research study. The present investigator anticipates no major risks or discomforts will occur in the current study. It is important however to recognize the following potential risks and discomforts that may be incurred.

1. There may be discomfort related to the delayed onset of muscle soreness associated with maximal contractions of the arm muscles. If muscle soreness does occur, it is usually very mild and should dissipate within 72 hours.
2. Maximal effort isometric contractions are associated with an increase in blood pressure. If you have received medical clearance and/or are already physically active, the risks are minimal. The researchers' first priority as an investigator is to maintain the emotional, psychological, and physical health of those participating in the study.

Steps to Mitigate Physical Risk:
During the study the participant must inform the researcher of any discomfort and the study will be stopped immediately. After the study the participants will be given stretches to complete to reduce the chance of delayed onset muscle soreness the next day. If soreness is experienced it should dissipate over the subsequent 24 hour period, but if it were to persist the participants will be recommended to inform the researchers and visit with their family physician immediately.

Potential Benefits
Participants will receive no direct benefits from participating in this study. However, participants should know that their willingness to serve as a participant for this experiment will allow us to

better predict strength capabilities during occupational upper extremity tasks, enabling us to reduce the risk of workplace injury.

Payment or Reimbursement
If you agree to take part, you will be financially compensated with $20 for the session.

Confidentiality
Your data will not be shared with anyone except with your consent or as required by law. All personal information such as your name, address, phone number or email will be removed from the data and will be replaced with a number. A list linking the number with your name will be kept in a secure place, separate from your file. The data, with identifying information removed will be securely stored in a locked office in the research office and on an encrypted hard drive. The data for this research study will be retained for ten years.

If the results of the study are published, your name will not be used and no information that discloses your identity will be released or published without your specific consent to the disclosure.

Participation and Withdrawal
Participation in this study is voluntary. Refusal to participate will not result in loss of access to any services or programs at McMaster University to which you are entitled. Simply inform the investigator, Spencer Savoie, of your intention to withdraw at any point during this study. Any data collected up until point of withdrawal will be destroyed unless your consent is given for us to keep the data. You may also refuse to answer any questions and still remain in the study. The investigator may withdraw you from this research if circumstances arise which warrant doing so.

Information about the Study Results
You may obtain information about the results of the study by contacting one of the investigators or by leaving your email address on a confidential form to which the final results will be sent. A brief summary of the results will be available approximately 4 months after data collection

Questions about the Study
If you have any questions about the research now or later, please contact Dr. Peter Keir at 905-525-9140, ext.23543 or Spencer Savoie at 905-525-9140, ext. 20175.

This study has been reviewed by the McMaster University Research Ethics Board and received ethics clearance.
If you have concerns or questions about your rights as a participant or about the way the study is conducted, please contact:

McMaster Research Ethics Secretariat
Telephone: (905) 525-9140 ext. 23142
c/o Research Office for Administrative Development and Support
E-mail: ethicsoffice@mcmaster.ca

CONSENT

- I have read the information presented in the letter of information/consent about a study being conducted by Dr. Peter Keir and Spencer Savoie of McMaster University.
- I have had the opportunity to ask questions about my involvement in this study and to receive additional details I requested.
- I understand that if I agree to participate in this study, I may withdraw from the study at any time.
- I have been given a copy of this form.
- I agree to participate in the study.

Signature: ______________________________________ Date: ____________

Name of Participant (Printed) ___________________________________

1. ____Yes, I would like to receive a summary of the study's results.
Please send them to this email address ____
Or to this mailing address: ____
____
____

… _____No, I do not want to receive a summary of the study's results.